Composite Structures 255 (2021) 112915

Contents lists available at ScienceDirect

Composite Structures

journal homepage: www.elsevier.com/locate/compstruct

Development of hybrid dimension adaptive sparse HDMR for stochastic finite element analysis of composite plate

Amit Kumar Rathi [a], Arunasis Chakraborty [b,*]

[a] Department of Civil and Infrastructure Engineering, Indian Institute of Technology Jodhpur, Jodhpur 342037, Rajasthan, India
[b] Department of Civil Engineering, Indian Institute of Technology Guwahati, Guwahati 781039, Assam, India

ARTICLE INFO

Keywords:
Uncertainty quantification
Reliability analysis and design
Dimension adaptiveness
High dimensional model representation
Kriging
Sparse grid

ABSTRACT

A novel adaptive high dimensional model representation (HDMR) is developed for stochastic finite element analysis of composite plate. Uncertainty propagating through the physical system is quantified using this technique where only the significant dimensions are retained. Influence of these dimensions is modeled by different orders which are preferred to be low for computational tractability. These dimensions are identified by a sensitivity analysis using support points in the sparse grid which are generated using multiple levels of hierarchy, joint or marginal probability distributions and dimension adaptiveness. This multi level hierarchical generation of support points fill the domain of the input variables with major emphasis on the regions of interest which may be the entire space, limit state, maxima/minima or tail ends of the probability distribution function for rare events depending upon the nature of the problem. The hybrid characteristics of the proposed dimension decomposition is introduced in this paper where the component functions are expressed using orthogonal bases and the error term which is further modeled using Gaussian random process (i.e. Kriging). The performance of the proposed *Hybrid* dimension adaptive HDMR (*hd*A-HDMR) is illustrated using stochastic finite element analysis of laminated composite plate whose material properties are considered as homogeneous non-normal random fields.

1. Introduction

Non-intrusive formulation is a substitution paradigm to quantify the input–output relationship between the variables of a physical system. Different modeling techniques for this purpose are available in the literatures [1–4] e.g. response surface method (RSM), polynomial chaos expansion (PCE), radial basis functions (RBF), neural networks, support vector regression (SVR), Kriging, high dimensional model representation (HDMR) etc. Their performances are usually influenced by the basis functions, support point generation scheme and discretization of the domain to develop the model. Here, the term *support points* refer to the locations where the original system are evaluated to train the artificial model. In stochastic computations, these methods aid in executing time consuming random realizations from population based methods such as Monte Carlo simulation (MCS), Latin hypercube samples (LHS) and so on. One of the popular methods for this purpose is PCE which uses orthogonal bases like Hermite, Laguerre, Jacobi and Legendre under the Askey scheme [5,6]. The unknown coefficients in this technique are evaluated using different fitting tools e.g. collocation [7,8], projection [9], least square regression (ordinary, weighted and moving) [10–14], least angle regression (LARS) [15] etc.

Different adaptive versions are proposed in the literatures to enhance their performance for stochastic computations using hyperbolic expansion and adaptive generation of basis terms [15,16]. Further improvement of its performance was proposed by Schobi et al. [17] using PCE coupled with Kriging. In their proposal, the original function was replicated by sparse PCE with truncation error modeled using Kriging. They incorporated hyperbolic expansion in order to limit the number of cross terms. Also, the adaptive generation of the bases were conducted by LARS to eliminate the ineffective bases in PCE. LHS was used to generate the support points to train the model in two different ways – considering LARS directly or screening one-by-one to get an optimal expansion. Application of this PCE-Kriging technique was limited to performance functions with low to moderate number of random variables (i.e. < 20) [18]. Using this technique, Dutta et al. [19] performed reliability based design optimization (RBDO) of thin tensile membrane structures exposed to uncertain wind loading. The dimension of the problem considered in their study was

* Corresponding author.
E-mail addresses: akrathi@iitj.ac.in (A.K. Rathi), arunasis@iitg.ac.in (A. Chakraborty).

https://doi.org/10.1016/j.compstruct.2020.112915
Received 29 July 2019; Revised 12 August 2020; Accepted 1 September 2020
Available online 10 September 2020

also low (i.e. 3). Zhang et al. [20] applied a sequential generation of the support points to improve the performance of Kriging based model. Support points were populated in the region of interest (e.g. near limit state for reliability analysis) using the probability of prediction from the model to identify the failure region. Haeri and Fadaee [21] extended the application of this scheme for reliability analysis of laminated composite plates. However, their study was limited to a high probability of failure (i.e. $> 10^{-2}$) with a moderate number of random variables (< 15). This emphasizes that non-intrusive models in the tail end region (i.e. low failure probability) for large dimensional problems remain an open area of future research.

Besides the development of PCE and Kriging, dimension decomposition (e.g. HDMR) [22] has also gained popularity in the recent past. It was developed using analysis of variance (ANOVA) for efficient representation of the performance function with the help of orthogonal subfunctions of lower dimensions [23–26]. It can accurately decouple a performance function to form the response surface. The support points in this technique are often generated using either random sampling (e.g. Sobol' sequence, LHS) [27,28] or deterministic points (e.g. mesh grids) [29]. The choice of the support point generation scheme leads to different formulation as the subfunctions change. Ziehn and Tomlin [27] proposed Sobol' sequence based HDMR formulation with modified Legendre polynomials as the bases to model the subfunctions. The bases were selected using sensitivity analysis with respect to output. This formulation was later adopted by Dey et al. [28,30] for uncertainty quantification of composite plates. Chakraborty and Chowdhury [31] proposed *hp* adaptive generalized ANOVA expansion based on optimal polynomial degree, number of support points and significant component functions. Chen et al. [32] used HDMR for Sobol sensitivity analysis of the stresses induced at the bolted joints in a composite plate. Ma and Zabaras [33] proposed adaptive finite difference HDMR using the sparse grid collocation to interpolate the component functions. Their numbers were restricted using significant dimensions based on sensitivity which resulted in limited sparse grid generation using Smolyak's algorithm. Using mesh grid points, Chowdhury et al. [22,34,35] proposed finite difference HDMR for efficient reliability analysis using moving least square (MLS) technique with regular polynomial bases. This new interpolation scheme proved to be efficient than the conventional Lagrange interpolation which was further improved by Rathi and Chakraborty [36] using PCE to model the subfunctions. They proposed multi HDMR formulation to enhance the quality of decomposition for reliability analysis. A dimension adaptive formulation was also suggested by Rathi and Chakraborty [36] for large problems using Pearson correlation coefficients. In addition to the advanced versions of HDMR, hybrid versions are also developed in the recent past. Yadav and Rahman [37] proposed a hybrid formulation using summand and multiplicative polynomial bases to represent the subfunctions of HDMR. They used it for uncertainty quantification of acoustics in a vehicle cabin with first order HDMR. Macías et al. [38] applied Kriging and HDMR to estimate the uncertainty in natural frequencies of the carbon nanotube composite plates. Recently, another hybrid formulation was suggested by Chakraborty and Chowdhury [39–42] using Kriging with randomly generated support points. They termed their dimension decomposition formulation as hybrid polynomial correlated function evaluation (H-PCFE). In this proposal, Kriging was applied on ad hoc basis for the global error approximation. Chatterjee and Chowdhury [43,44] extended this formulation for uncertainty quantification of offshore structures. The unknown coefficients were determined using SVR while Bayesian learning was adapted for better training of the meta-model. Contrary to this global error modeling, Ulaganathan et al. [45] applied gradient enhanced Kriging to model the errors in the subfunctions of HDMR. They demonstrated the performance of their hybrid technique using different support point generation schemes involving LHS, Voronoi partition and maximin sampling. However, the examples illustrated by them were corresponding to the fitting error of the proposed meta-model technique which requires further investigation with respect to its application in stochastic computations.

1.1. Objectives of this study and problem formulation

Aforementioned literature review shows the chronological development of dimension decomposition with major emphasis on HDMR and its advanced versions for the solution of large dimensional problems (e.g. composite plates with spatial variability). These research works are mainly focused on various modifications in terms of bases, component functions and unknown coefficients in the formulation. These modifications include MLS [22,34–36] which employs evolving coefficients to minimize the error at individual locations with respect to the assumed weight function. Hence, making the proposed formulation scalar in the sense that each realization needs to be solved independently, eventually results in multiple matrix inversions for uncertainty quantification and reliability analysis. This issue exponentially escalates the computational cost when the dimension of the problem is high. Also, inversion of large matrices cause ill-conditioning which result in erroneous modeling. Based on this discussion, following are the objectives set for the present study.

- Develop a hybrid dimension adaptive decomposition of the performance function with multiple generation of HDMRs for uncertainty quantification of composite structures.
- Estimate the probability of failure by accurate and efficient representation of the limit state, especially near the region of interests.
- Improve the computational cost to solve the reliability based design problem involving large number of random variables for optimal solution.

These objectives are addressed in this paper where a new formulation of hybrid dimension adaptive (*d*-Adaptive) HDMR is proposed. Besides matrix inversion, the error term in this proposal is modeled as a random process. This adaptive sparse formulation of HDMR is based on the significance of the dimension. Thus, the model presented in this paper uses the apt combination of *d*-Adaptive formulation with multiple generations of the HDMR. Here, the error is also modeled as a Gaussian random process along with the adaptive sparse formulation of HDMR for more accurate local approximation. This coupling of the multiple dimension decompositions and the error modeling using random process (i.e. Kriging) leads to a formulation with polynomial bases and weigh functions. These terms can be referred a parametric and nonparametric based on their nature of the application, respectively. Hence, it makes the proposal hybrid for dimension decomposition. It is applied to solve different problems in stochastic computation which includes accurate estimation of the probability of failure by a near exact representation of the limit state, especially near the most probable failure point (MPP). It also improves the computational cost of a reliability based design problem with large number of random variables for optimal solution. In this paper, the application of the proposed method is demonstrated for stochastic finite element analysis of composite plate with different support conditions when exposed to spatial randomness in material properties. The mathematical framework of the proposed hybrid HDMR is discussed in the following section.

2. Development of hybrid *d*-Adaptive HDMR

In this section, formulation of the proposed *d*-Adaptive HDMR is presented to model the input–output relation of large dimensional problems. An example with a few random variables is added in the Appendix A for further clarity. In general, this relation involves lower order influences of the input variables for a well-defined physical sys-

tem [46]. The proposal uses this characteristic for hierarchical decomposition of the original function, thus making it robust for reliability analysis and uncertainty quantification.

Let a physical system or model which yields an output $g(\mathbf{x})$ is subjected to a n-dimensional vector of input variables represented by $\mathbf{x}$ where the performance function can be expressed in the following form

$$g(x_1,x_2,\ldots,x_n) = g_0 + \sum_{1\leqslant i_1\leqslant n} g_{i_1}(x_{i_1}) + \sum_{1\leqslant i_1<i_2\leqslant n} g_{i_1 i_2}(x_{i_1},x_{i_2}) + \cdots + \sum_{1\leqslant i_1<i_2<\cdots<i_j\leqslant n} g_{i_1 i_2\ldots i_j}\left(x_{i_1},x_{i_2},\ldots,x_{i_j}\right) + \cdots + g_{12\ldots n}(x_1,x_2,\ldots,x_n) \quad (1)$$

The above expression gives a hierarchical expansion of $g(\mathbf{x})$ in terms of sub-functions which are based on their association with the number of random variables as shown in Fig. 1a. The notations $g_0, g_{i_1}(x_{i_1}), g_{i_1 i_2}(x_{i_1},x_{i_2}), g_{i_1 i_2\ldots i_j}\left(x_{i_1},x_{i_2},\ldots,x_{i_j}\right)$ and $g_{12\ldots n}(x_1,x_2,\ldots,x_n)$ represent mean component, influence due to x_{i_1}, (x_{i_1},x_{i_2}), $(x_{i_1},x_{i_2},\ldots,x_{i_j})$, $(x_{i_1},x_{i_2},\ldots,x_{i_n})$, respectively. Symbolically, the number of component functions in the jth order is given by $\binom{n}{j}$. Here, it may be noted that the higher order components in Eq. (1) can be insignificant and hence, they are neglected for computational efficiency. Thus, only limited lower order terms are considered for accurate and efficient determination of the output. This truncation typically proves to be adequate for practical problems, however, it does not undermines the significance of any higher order term in Eq. (1). The importance of a particular order is specific to the problem which can be determined based on the sensitivity analysis (e.g. Sobol' sensitivity indices). This, in turn, makes the formulation adaptive where only important terms are retained for further analysis. This procedure (i.e. sensitivity analysis) demand significant computational cost which in this paper is alleviated by an efficient hybrid d-Adaptive approach as explained below.

Suppose, a few input variables in $\mathbf{x}$ are significant (*viz.* $x_{i_1},x_{i_2},\ldots,x_{i_{n_r}}$) to the output whose indices $\{i_1,i_2,\ldots,i_{n_r}\}\in N_{n_r}$ form a subset of $N_n=\{1,2,\ldots,n\}$. The component functions associated with the insignificant variables (i.e. $x_i, \forall i\in N_n \setminus N_{n_r}$) constitute a residual term $\hat{\mathcal{R}}_{n_r}$. This residual is neglected in the HDMR formulation without loss of accuracy for all practical purpose. It leads to the curtailment of the expansion in Eq. (1) as shown in Fig. 1b where the insignificant variables are removed to save the computational cost. Hence, the basic dimension curtailed formulation of the HDMR is given by

$$g(\mathbf{x}) = g_0 + \sum_{i_1\in N_{n_r}} g_{i_1}(x_{i_1}) + \sum_{\substack{i_1,i_2\in N_{n_r}\\ i_1<i_2}} g_{i_1 i_2}(x_{i_1},x_{i_2}) + \cdots + \sum_{\substack{i_1,i_2,\ldots,i_j\in N_{n_r}\\ i_1<i_2<\cdots<i_j}} g_{i_1 i_2\ldots i_j}\left(x_{i_1},x_{i_2},\ldots,x_{i_j}\right) + \cdots + g_{i_1 i_2\ldots i_{n_r}}(x_{i_1},x_{i_2},\ldots,x_{n_r}) + \hat{\mathcal{R}}_{n_r} \quad (2)$$

In this paper, finite difference HDMR is used with a reference point (or anchor point) through which hyper-planes are constructed. Let $\mathbf{c}=\{c_{i_1}\ c_{i_2}\ \cdots\ c_{n_r}\}$ be this point to construct the component functions. As a practical choice, the reference point is often set to the mean values $\mu_{\mathbf{x}}$ of the input variables. The component functions are determined by the formation of the hypothetical planes through $\mathbf{c}$ which cuts the function for an accurate representation. This results in a sequential evaluation of the component functions as

$$\begin{aligned} g_0 &= g(\mathbf{c}), \quad g_{i_1}(x_{i_1}) = g(\mathbf{c}_{i_1},x_{i_1}) - g_0, \quad g_{i_1 i_2}(x_{i_1},x_{i_2}) \\ &= g(\mathbf{c}_{i_1 i_2},x_{i_1},x_{i_2}) - g_{i_1}(x_{i_1}) - g_{i_2}(x_{i_2}) - g_0 \end{aligned} \quad (3)$$

and so on, where $g(\mathbf{c}_{i_1},x_{i_1})$ and $g(\mathbf{c}_{i_1 i_2},x_{i_1},x_{i_2})$ denote the subfunctions $g(x_{i_1},c_{i_2},\ldots,c_{n_r})$ and $g(x_{i_1},x_{i_2},c_{i_3},\ldots,c_{n_r})$, respectively. In the subfunctions, the coordinates of all the input variables are locked at the reference point except for the specific input variables which are mentioned in the brackets. Similarly, the notations can be extended for the other component functions of the HDMR expansion. These component functions are subtracted by the preceding orders (as in Eq. 3) to assure the exclusive contribution of that order in the expansion. Substituting Eq. (3) till 1st order terms back in Eq. (2) leads to

$$g(\mathbf{x}) = \sum_{i_1\in N_{n_r}} g(\mathbf{c}_{i_1},x_{i_1}) - (n_r-1)g(\mathbf{c}) + \hat{\mathcal{R}}_1 \quad (4)$$

where, $\hat{\mathcal{R}}_1$ is the residual contribution of all orders above 1. The bivariate contributions of the input variables are presented by the 2nd order component function $g_{i_1 i_2}(x_{i_1},x_{i_2})$. These are determined by a surface, cut through the variable space defined by x_{i_1} and x_{i_2} at a location $\mathbf{c}$. Hence, the 2nd order dimension curtailed HDMR expansion can be obtained following the similar process

$$g(\mathbf{x}) = \sum_{\substack{i_1,i_2\in N_{n_r}\\ i_1<i_2}} g(\mathbf{c}_{i_1 i_2},x_{i_1},x_{i_2}) - (n_r-2)\sum_{i_1\in N_{n_r}} g(\mathbf{c}_{i_1},x_{i_1}) + \frac{(n_r-1)(n_r-2)}{2}g(\mathbf{c}) + \hat{\mathcal{R}}_2 \quad (5)$$

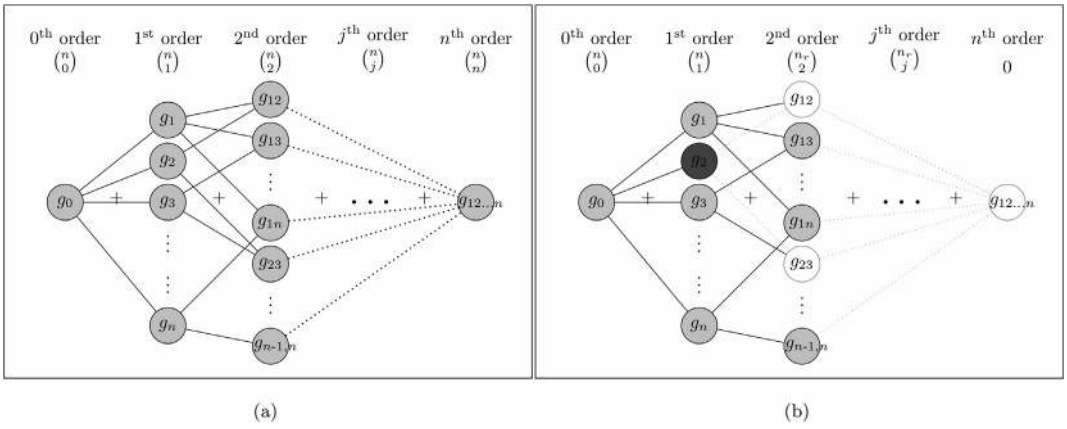

Fig. 1. Schematic representation of hierarchy in HDMR in terms of component functions for (a) complete formulation with n variables and (b) sparse formulation as per d-Adaptive proposal where only variable x_2 is screened as insignificant such that $n_r=n-1$ (highlighted by dark grey colour). The number of component functions in each order is calculated by binomial operator as specified and for simplicity $g(x_i)$ is denoted by g_i.

where, the notation $\hat{\mathcal{R}}_2$ represents the residual in 2nd order HDMR. The above expressions (i.e. Eqs. (4) and (5)) explicitly eliminate the contributions of all the insignificant dimensions from the expansion. However, in the present study, it is proposed to use 1st order with all the random variables and thereon, the dimensions are curtailed from 2nd order onward. This intermittency is recommended for practical purpose as it reduces the number of component functions which increases with the order. Hence, the new dimension curtailed expansion is given as

$$\begin{aligned} g(\mathbf{x}) \quad = & \sum_{\substack{i_1,i_2 \in N_{n_r} \\ i_1 < i_2}} g(\mathbf{c}_{i_1 i_2}, x_{i_1}, x_{i_2}) - (n_r - 1) \sum_{i_1 \in N_{n_r}} g(\mathbf{c}_{i_1}, x_{i_1}) \\ & + \sum_{i_1 \in N_n} g(\mathbf{c}_{i_1}, x_{i_1}) + \left\{ \tfrac{n_r(n_r-1)}{2} - (n-1) \right\} g(\mathbf{c}) + \acute{\mathcal{R}}_2 \end{aligned} \tag{6}$$

The residual in this expansion is represented by $\acute{\mathcal{R}}_2$. The above expansion can also be expressed in the compact for $g(\mathbf{x}) = \tilde{g}(\mathbf{x}) + \acute{\mathcal{R}}$, where $\tilde{g}(\mathbf{x})$ is the approximation without the residual influence. Also, this expression is subjected to evaluation of $g(\bullet)$ at only the reference point $\mathbf{c}$ and the support points around it. Hence, to determine the output at any arbitrary point $\mathbf{x}$, the expansion in Eq. (6) is modified as

$$\begin{aligned} \tilde{g}(\mathbf{x}) \quad = & \sum_{\substack{i_1,i_2 \in N_{n_r} \\ i_1 < i_2}} y_{i_1 i_2}(\mathbf{c}_{i_1 i_2}, x_{i_1}, x_{i_2}) - (n_r - 1) \sum_{i_1 \in N_{n_r}} y_{i_1}(\mathbf{c}_{i_1}, x_{i_1}) \\ & + \sum_{i_1 \in N_n} y_{i_1}(\mathbf{c}_{i_1}, x_{i_1}) + \left\{ \tfrac{n_r(n_r-1)}{2} - (n-1) \right\} y_0 \end{aligned} \tag{7}$$

In this context, the sensitivity analyses to identify the important input variables are performed using Pearson correlation coefficient which is defined by

$$\rho_{gx_i} = \frac{\mathbb{E}[(g - \mathbb{E}[g])(x_i - \mathbb{E}[x_i])]}{\sqrt{\mathbb{E}\left[(g - \mathbb{E}[g])^2\right] \ \mathbb{E}\left[(x_i - \mathbb{E}[x_i])^2\right]}}, \quad \forall i \in N_n \tag{8}$$

as suggested by Rathi and Chakraborty [36]. In the above expression, the correlation coefficients ρ_{gx_i} are evaluated to detect the importance of that particular variable. It may be noted that the proposed formulation is applicable with any other sensitivity analysis to determine the significant dimension by employing other techniques available in the literature [27,28,33,47–49].

Once the significant variables are selected, associated unknown terms are represented by the subfunctions of $g(\mathbf{x})$. In this paper, these terms are expressed by truncated PCE for local approximation. This secondary representation of each component function is required to determine the response at any arbitrary point based on the values at the support points. Earlier, the coefficients associated with the PCE were used to address the local approximation using the MLS technique as suggested by Rathi and Chakraborty [36]. Application of MLS incurred a scalar approach which leads to the independent determination of the unknown coefficients at each realization. This issue is addressed by introducing additional nonparametric terms [i.e. $U(\bullet)$] in each cut made by finite difference-HDMR under the proposed formulation. Hence, the secondary approximation in each component function is represented by

$$\begin{aligned} y_k(\bullet) \quad = & \alpha_0 \Gamma_0 + \sum_{i_1 \in k} \alpha_{i_1} \Gamma_1(z_{i_1}) + \sum_{i_1, i_2 \in k} \alpha_{i_1 i_2} \Gamma_2(z_{i_1}, z_{i_2}) + \cdots \\ & + \sum_{i_1, i_2, \ldots, i_p \in k} \alpha_{i_1 i_2 \ldots i_p} \Gamma_p(z_{i_1}, z_{i_2}, \ldots, z_{i_p}) + \underbrace{\textstyle\sum_{1 \leqslant j \leqslant n_s} \beta_j R_k(\mathbf{z}, \mathbf{z}^j)}_{U_k(\bullet)} \end{aligned} \tag{9}$$

Here, the notation k represents the associated indices $i_1, i_2, \ldots, i_{n_r}, i_1 i_2, \ldots, i_{n_r - 1} i_{n_r}$ as per Eq. (7) in a set and p denotes the degree of orthogonal polynomial bases Γ_p. Previous literatures [5,6,12] suggest various orthogonal bases Γ as per Askey scheme which can be adopted in this formulation. However, Hermite polynomial bases are used in this study which is given below

$$\Gamma_p(z_{i_1}, z_{i_2}, \ldots, z_{i_p}) = \exp\left(\frac{1}{2}\mathbf{z}\mathbf{z}^\top\right)(-1)^p \frac{\partial^p \exp\left(-\frac{1}{2}\mathbf{z}\mathbf{z}^\top\right)}{\partial z_{i_1} \partial z_{i_2} \cdots \partial z_{i_p}} \tag{10}$$

where, $\mathbf{z} = \{z_{i_1}\, z_{i_2} \ \ldots \ z_{i_p}\}$ such that $\mathbf{\Gamma}_0 = 1, \mathbb{E}[\mathbf{\Gamma}_{i_1}] = 0$ and $\mathbb{E}[\mathbf{\Gamma}_{i_1}\mathbf{\Gamma}_{i_2}] = \delta_{i_1 i_2}$. The notations $\mathbb{E}$ and δ represent the expectation operator and Kronecker delta function, respectively. The unknown coefficients associated to theses bases in Eq. 9 are $\alpha_0, \alpha_{i_1}, \alpha_{i_1 i_2}, \ \ldots, \ \alpha_{i_1 i_2 \ldots i_p}$ and the variable z is Gaussian with $\mathcal{N}(0,1)$. This discretization is also helpful as it can be directly adopted for random fields modeled by Karhunen-Loève transformation as both are in the standard normal space. Moreover, this formulation can be extended for different distributions with dependent random variables using standard transformation techniques e.g. Rosenblatt transformation [50] or Nataf model [51]. These features can be accommodated in the proposed framework as it provides adequate flexibility.

Here, it may be noted that in this formulation, the component functions includes nonparametric terms $U_k(\bullet)$ in PCE framework. It helps to capture the influence of n_s support points based on the unknown coefficient β_j and weight function $R_k(\mathbf{z}, \mathbf{z}^j)$ in the variable space. In the weight function, $\mathbf{z}, \mathbf{z}^j$ denote the outcomes at prediction location and jth support points, respectively. Different weight functions exist in the literature for this purpose e.g. linear, cubic, spline, exponential, Gaussian etc. [52]. In this study, the nonparametric term $U_k(\bullet)$ is assumed to be Gaussian with zero mean and $\sigma_k^2 R_k(\mathbf{z}^I, \mathbf{z}^J)$ as the covariance, where σ_k is the standard deviation. On simplification, Eq. (9) can be rewritten as

$$y_k(\bullet) = \mathbf{\Gamma}_k(\bullet)^\top \boldsymbol{\alpha}_k^* + \mathbf{r}_k(\bullet)^\top \boldsymbol{\beta}_k^* \tag{11}$$

which is substituted back into Eq. (7) to get the proposed hybrid formulation of the d-Adaptive HDMR in the following format

$$\begin{aligned} \tilde{g}(\mathbf{x}) = & \sum_{\substack{i_1,i_2 \in N_{n_r} \\ i_1 < i_2}} \mathbf{\Gamma}_{i_1 i_2}(x_{i_1}, x_{i_2})^\top \boldsymbol{\alpha}_{i_1 i_2}^* - (n_r - 1) \sum_{i_1 \in N_{n_r}} \mathbf{\Gamma}_{i_1}(x_{i_1})^\top \boldsymbol{\alpha}_{i_1}^* \\ & + \sum_{i_1 \in N_n} \mathbf{\Gamma}_{i_1}(x_{i_1})^\top \boldsymbol{\alpha}_{i_1}^* \\ & + \underbrace{\begin{array}{l} \textstyle\sum_{\substack{i_1,i_2 \in N_{n_r} \\ i_1 < i_2}} \mathbf{r}_{i_1 i_2}(x_{i_1}, x_{i_2})^\top \boldsymbol{\beta}_{i_1 i_2}^* \\ -(n_r - 1) \textstyle\sum_{i_1 \in N_{n_r}} \mathbf{r}_{i_1}(x_{i_1})^\top \boldsymbol{\beta}_{i_1}^* + \sum_{i_1 \in N_n} \mathbf{r}_{i_1}(x_{i_1})^\top \boldsymbol{\beta}_{i_1}^* \end{array}}_{\text{proposed } \textit{hybrid} \text{ formulation}} \\ & + \left\{ \tfrac{n_r(n_r-1)}{2} - (n-1) \right\} \mathbf{\Gamma}_0^\top \boldsymbol{\alpha}_0^* \end{aligned} \tag{12}$$

Expanding the above equation gives the complete expression for the proposed *hd*A-HDMR which takes the following form

$$\begin{aligned} \tilde{g}(\mathbf{x}) \quad = & \sum_{j_1=1}^{n_r - 1} \sum_{j_2 > j_1}^{n_r} \left[\sum_{k_2=0}^{p} \left\{ \sum_{l_1=1}^{2} \cdots \sum_{l_{k_2}=1}^{l_{(k_2-1)}} \alpha_{i_{j_1} \ldots i_{j_{k_2}}} \Gamma_{k_2}\left(z_{i_{j_1}}, \ldots, z_{i_{j_{k_2}}}\right) \right\} \right] \\ & - (n_r - 1) \sum_{j_1=1}^{n_r} \left\{ \sum_{k_1=0}^{p} \alpha_{i_{j_1} k_1} \Gamma_{k_1}(z_{j_1}) \right\} + \sum_{j_1=1}^{n} \left\{ \sum_{k_1=0}^{p} \alpha_{i_{j_1} k_1} \Gamma_{k_1}(z_{j_1}) \right\} \\ & + \sum_{j_1=1}^{n_r - 1} \sum_{j_2 > j_1}^{n_r} \left[\sum_{m_2=1}^{n_s} \beta_{m_2} R_{i_{j_1} i_{j_2}}(\mathbf{z}, \mathbf{z}^{m_2}) \right] - (n_r - 1) \sum_{j_1=1}^{n_r} \left[\sum_{m_1=1}^{n_s} \beta_{m_1} R_{i_{j_1}}(\mathbf{z}, \mathbf{z}^{m_1}) \right] \\ & + \sum_{j_1=1}^{n} \left[\sum_{m_1=1}^{n_s} \beta_{m_1} R_{i_{j_1}}(\mathbf{z}, \mathbf{z}^{m_1}) \right] + \left\{ \tfrac{n_r(n_r-1)}{2} - (n-1) \right\} \alpha_0 \Gamma_0 \end{aligned} \tag{13}$$

It can be noted that the above formulation in Eq. (13) is constructed for a single decomposition around the reference point. However, the present study proposes an iterative scheme for efficient support point generation around multiple reference points. In this regard, multiple

HDMRs are constructed over these reference points. The contribution of each HDMR is summarized as

$$\tilde{g}(\mathbf{x}) = \sum_{i=1}^{it} \gamma^{(i)}(\mathbf{x}, \mathbf{c}^{(i)}) \tilde{g}^{(i)}(\mathbf{x}) \tag{14}$$

where, *it* is the number of iterations. These multiple generations also provide flexibility by incorporating different polynomial degree p and order o for individual HDMR. A typical example of this can be explained using two different orders, say 1st and 2nd orders, in different iterations. Here, the first iteration utilizes 2nd order model whereas successive iterations use 1st order. This is applied to limit the generation of support points and subsequently, the computational effort without loss of accuracy as suggested in Rathi and Chakraborty [36]. Thus, the *hd*A-HDMR formulation is expressed by

$$\begin{aligned}
\tilde{g}(\mathbf{x}) = {} & \gamma^{(1)}(\mathbf{x}, \mathbf{c}^{(1)}) \left[\sum_{j_1=1}^{n_r-1} \sum_{j_2>j_1}^{n_r} \left[\sum_{k_2=0}^{p^{(1)}} \left\{ \sum_{l_1=1}^{2} \cdots \sum_{l_{k_2}=1}^{l_{(k_2-1)}} \alpha^{(1)}_{i_{j_{l_1}} \cdots i_{j_{l_{k_2}}}} \Gamma^{(1)}_{k_2}(z_{i_{j_{l_1}}}, \ldots, z_{i_{j_{l_{k_2}}}}) \right\} \right] \right. \\
& - (n_r - 1) \sum_{j_1=1}^{n_r} \left\{ \sum_{k_1=0}^{p^{(1)}} \alpha^{(1)}_{i_{j_1}, k_1} \Gamma^{(1)}_{k_1}(z_{i_{j_1}}) \right\} + \sum_{j_1=1}^{n} \left\{ \sum_{k_1=0}^{p^{(1)}} \alpha^{(1)}_{i_{j_1}, k_1} \Gamma^{(1)}_{k_1}(z_{i_{j_1}}) \right\} \\
& + \sum_{j_1=1}^{n_r-1} \sum_{j_2>j_1}^{n_r} \left[\sum_{m_2=1}^{n_s^{(1)}} \beta^{(1)}_{m_2} R^{(1)}_{i_{j_1} i_{j_2}}(\mathbf{z}, \mathbf{z}^{m_2}) \right] - (n_r - 1) \sum_{j_1=1}^{n_r} \left[\sum_{m_1=1}^{n_s^{(1)}} \beta^{(1)}_{m_1} R^{(1)}_{i_{j_1}}(\mathbf{z}, \mathbf{z}^{m_1}) \right] \\
& + \sum_{j_1=1}^{n} \left[\sum_{m_1=1}^{n_s^{(1)}} \beta^{(1)}_{m_1} R^{(1)}_{i_{j_1}}(\mathbf{z}, \mathbf{z}^{m_1}) \right] + \left\{ \frac{n_r(n_r-1)}{2} - (n-1) \right\} \alpha^{(1)}_0 \Gamma^{(1)}_0 \Big] \\
& + \sum_{i=2}^{it} \gamma^{(i)}(\mathbf{x}, \mathbf{c}^{(i)}) \left[\sum_{j_1=1}^{n_r} \left\{ \sum_{k_1=0}^{p^{(i)}} \alpha^{(i)}_{i_{j_1}, k_1} \Gamma^{(i)}_{k_1}(z_{i_{j_1}}) \right\} + \sum_{j_1=1}^{n_r} \left[\sum_{m_1=1}^{n_s^{(i)}} \beta^{(i)}_{m_1} R^{(i)}_{i_{j_1}}(\mathbf{z}, \mathbf{z}^{m_1}) \right] + (n_r - 1) \alpha^{(i)}_0 \Gamma^{(i)}_0 \right]
\end{aligned} \tag{15}$$

here, the superscript in parentheses denotes the iteration, such that $R^{(i)}_{i_{j_1} i_{j_2}}$ represents the weight term $R_\bullet$ of the component function $y_{i_{j_1} i_{j_2}}$ with variables $z_{i_{j_1}}$ and $z_{i_{j_2}}$ for ith iteration. It may be noted that highlighted terms in the above equation constitute the proposed hybrid dimension decomposition formulation. The use of lower orders in this expression is not restricted and the influence of higher order HDMR can be easily incorporated extending the sequence shown in Eq. (3). The degree p of the orthogonal bases in PCE can be either chosen by the designer or selected based on the number of support points n_s available for its complete generation. The unknown coefficients, $\alpha^{(\bullet)}_\bullet, \beta^{(\bullet)}_\bullet$ and $\gamma^{(\bullet)}$, in the above equation are determined utilizing the support points which are discussed in the following section.

2.1. Determination of unknown coefficients

In this study, the unknown quantities in Eq. (15) are characterized in three categories based on their evaluation strategies. A steps-wise evaluation of these coefficients are given below -.

Step 1: The unknown coefficients $\alpha^{(\bullet)}_\bullet$ associated to the orthogonal bases are evaluated using mean square error between the PCE and the original values. It is minimized using best linear unbiased prediction (BLUP) [53–55] as in Kriging which is similar to MLS technique [36] for unbiased prediction. Using this optimization, the coefficients are determined as

$$\boldsymbol{\alpha}_\bullet = \left[\boldsymbol{\Gamma}^{\mathrm{T}}(\bullet) \mathbf{R}^{-1} \boldsymbol{\Gamma}(\bullet) \right]^{-1} \boldsymbol{\Gamma}^{\mathrm{T}}(\bullet) \mathbf{R}^{-1} \underline{\mathbf{g}}(\bullet) \tag{16}$$

where, $\underline{\mathbf{g}}_k = \left[\underline{g}_k(\mathbf{x}^1)\ \underline{g}_k(\mathbf{x}^2)\ \ldots\ \underline{g}_k(\mathbf{x}^{n_s}) \right]^{\mathrm{T}} \in \mathbb{R}^{n_s \times n_g}$ is the normalized output such that $\underline{g}_k(\bullet) = \left[g_k(\bullet) - \mu^g_k \right] / \sigma^g_k$ and n_g is the dimension of the output. The notations μ^g_k and σ^g_k are calculated as follows

$$\mu^g_k = \frac{1}{n_s} \sum_{i_1=1}^{n_s} g_k(\bullet^{i_1}) \tag{17a}$$

$$\sigma^g_k = \sqrt{\frac{1}{n_s} \sum_{i_1=1}^{n_s} \left(g_k(\bullet^{i_1}) - \mu^g_k \right)^2} \tag{17b}$$

Further, the polynomial bases in Eq. (16) are presented as $\boldsymbol{\Gamma}_k = [\Gamma_k(\mathbf{z}^1)\ \Gamma_k(\mathbf{z}^2)\ \ldots\ \Gamma_k(\mathbf{z}^{n_s})]^{\mathrm{T}} \in \mathbb{R}^{n_s \times n_b}$ and the weight matrix $\mathbf{R}_k \in \mathbb{R}^{n_s \times n_s}$ is formed as $\mathbf{R}^{ij}_k = R_k(\mathbf{x}^i, \mathbf{x}^j), i, j = 1, 2, \ldots, n_s$, where $\mathbf{r}_k(\mathbf{x}) = [R_k(\mathbf{x}, \mathbf{x}^1)\ R_k(\mathbf{x}, \mathbf{x}^2)\ \ldots\ R_k(\mathbf{x}, \mathbf{x}^{n_s})]^{\mathrm{T}}$ and the weigh structure evaluated using Gaussian expression follows

$$R_k(\mathbf{z}^I, \mathbf{z}^J) = \prod_{i=1}^{n} \exp\left[-\hat{\theta}_i \left(z^I_i - z^J_i \right)^2 \right] \tag{18}$$

In this study, the value of $\hat{\theta}_i$ is adopted as 0.75 for all the variables in the upcoming numerical analysis. The selection of this value depends on the designer and it is not decided based on any prior sensitivity analysis. The authors envisage that such ad hoc sensitivity analysis will not influence the proof of concept established here. However, the present study does not restrict its evaluation using the sensitivity of $\hat{\theta}$ on the output which can be performed as a separate study.

Step 2: Next, the coefficients $\beta^{(\bullet)}_\bullet$ associated with the nonparametric terms are determined utilizing the solution strategy involved in Step 1 as

$$\boldsymbol{\beta}_\bullet = \mathbf{R}^{-1} \left[\underline{\mathbf{g}}(\bullet) - \boldsymbol{\Gamma}(\bullet) \boldsymbol{\alpha}_\bullet \right] \tag{19}$$

Step 3: Since, all the unknown coefficients in $\alpha_{\bullet}^{(\bullet)}$ and $\beta_{\bullet}^{(\bullet)}$ are determined in the previous two steps, Eq. (13) is applied to construct the individual HDMRs. Finally, the individual contribution of these HDMRs are evaluated as

$$\gamma^{(i)} = \frac{\prod_{j=1,\, j\neq i}^{it} \sqrt{\sum_{k=1}^{n}\left(x_k - c_k^{(j)}\right)^2}}{\sum_{o=1}^{it}\prod_{l=1,\, l\neq o}^{it}\left[\sum_{k=1}^{n}\left(x_k - c_k^{l}\right)^2\right]^{\frac{1}{2}}} \tag{20}$$

where, $\sum_{i=1}^{it}\gamma^{(i)} = 1$. It can be noted that similar to the above two steps, $\gamma^{(\bullet)}$ also utilizes the location of the arbitrary point. That apart, the determination of this coefficient considers the reference point of the HDMR to ascertain its influence. It justifies the adaptive nature introduced by γ based on the proximity of HDMR w.r.t. the arbitrary point where the approximation is evaluated. It helps in a better fit, especially when mapping the local variations of the original function.

To calculate these coefficients, the present study employs distribution adaptive multi-sparse grid scheme which uses Smolyak's algorithm [56] and follows multiple HDMR decompositions to give an efficient sparse generation of the support points. The application of Smolyak's algorithm results in curtailment of the full-grid interpolation, thus improving the computational tractability. In the present formulation, the generation of support points require a dimension-wise adaptive formulation which is given by

$$\Delta\mathscr{H}_{q,n}(g) = \bigcup_{|\mathbf{i}|_1 = q-n+1} \left(x_{1,\Delta}^{(i_1)} \otimes x_{2,\Delta}^{(i_2)} \otimes \ldots \otimes x_{n,\Delta}^{(i_n)}\right) \quad \boxed{\sum i_j \leq q_{nr},\ \forall j \in N_n \setminus N_{n_r}} \tag{21}$$

where, $x_{\bullet,\Delta}^{(i_l)} = x_{\bullet}^{(i_l)} \setminus x_{\bullet}^{(i_l-1)}$ with $x^{(0)} = \varnothing$, q is the level of sparse grid generation and q_{nr} is the level for insignificant random variables. Furthermore, in Eq. 21, $|\mathbf{i}|_1 = \sum_{k=1}^{n} i_k$ is the summation of hierarchies denoted by i_k for kth random variable. $\Delta\mathcal{H}_{q,n}$ gives the locations of the support points generated exclusively at level q using tensor product. These locations are determined in a unit space (i.e. $\mathbb{N}^n$) as follows

$$x^{(i,j)} = \begin{cases} 0.5 & \forall j = 1 \quad \text{when } n_{si} = 1 \\ \frac{j-1}{n_{si}-1} & \forall j = 1\ldots, n_{si} \quad \text{if } n_{si} > 1 \end{cases} \tag{22}$$

which can be linearly transformed to the original domain $\Omega_{\mathbf{x}}$. In the above equation, number of grid points n_{si} in ith hierarchy is calculated by

$$n_{si} = \begin{cases} 1 & \text{if } i = 1 \\ 2^{i-1}+1 & \forall i > 1 \end{cases} \tag{23}$$

This ultimately forms a dendriform as illustrated in Fig. 2a which starts with a centre point and fills the domain in successive levels. In the present study, the centre point reflects the reference point $\mathbf{c}$ in each iteration around which the other points are placed. The locations are generated using $\mathcal{H}_{q,n} = \bigcup_{i\leq q}\Delta\mathcal{H}_{i,n}$ such that all the levels within q are considered for the support points. A 2D system with variables x_1 and x_2 is illustrated for visualization of the generation scheme adopted in the present paper. Two cases are considered where the first case has both random variables as significant and in the other case, one random variable is insignificant. Fig. 2b and 2c gives the exclusive generation of supports points in each hierarchical level of the sparse grid. Here, the individual hierarchal indices for x_1 and x_2 (i.e. i_1 and i_2, respectively) are assigned as 1, 2, …, 5 for demonstration and the coordinates are evaluated using Eq. (22) in the unit space. In the sparse grid, support points are selected based on the ℓ_1 norm of the hierarchal indices vector $\mathbf{i}$ and sparse grid q as in Eq. (21). Fig. 2b shows the selected indices based on its summation for different levels of q which are denoted by • in the plot. In the second case, the support points are generated using an additional constraint shown in the box (see Eq. (21)) to limit the locations of the neglected random variable. Thus, another ℓ_1 norm is introduced exclusively for the neglected random variable. For demonstration purpose, the level q_{nr} is considered as 3 in this example. This results in the equal generation of point for both the cases till the sparse grid level is 3. Thereon, only the hierarchal indices in the x_1 (i.e. significant random variable) direction are selected to generate the locations. Subsequently, the number of support points generated in case 2 is less than case 1 as shown in Fig. 2c. This is particularly helpful in curtailing the curse of dimensionality in large problems as the space filling scheme is adaptive with respect to the sensitivity of the dimension.

In the present paper, the proposed method is applied to uncertainty quantification, reliability analysis and design optimization of the composite plate with spatial randomness. The stochastic FE formulation used in this study and the application of the proposed *hd*A-HDMR for uncertainty quantification are discussed in the following sections.

3. Stochastic FE formulation of composite plate

The stochastic FE analysis of the laminated composite plate shown in Fig. 3 is discussed in this section. For simplicity, a square composite plate of unit length is considered with uniformly thick plies (i.e. h_c/n_m, where n_m is number of piles). As shown in this figure, the geometric axes involved in this analysis are denoted as $\hat{x}, \hat{y}$ and $\hat{z}$ with mid-plane of the plate lying in $\hat{x}$–$\hat{y}$ axes. The deflections along these axes are evaluated using first order shear deformation theory (FSDT) [57]

$$\begin{aligned} u(\hat{x},\hat{y},\hat{z}) &= u_0(\hat{x},\hat{y}) + \hat{z}\phi_{\hat{x}}(\hat{x},\hat{y}) \\ v(\hat{x},\hat{y},\hat{z}) &= v_0(\hat{x},\hat{y}) + \hat{z}\phi_{\hat{y}}(\hat{x},\hat{y}) \\ w(\hat{x},\hat{y},\hat{z}) &= w_0(\hat{x},\hat{y}) \end{aligned} \tag{24}$$

In the above equation, $u_0,\ v_0,\ w_0$ are the mid-plane displacements and $\phi_{\bullet}(\hat{x},\hat{y})$ represents the rotation about the associated axis. Using the potential energy approach, the stiffness matrix of the laminated composite plate can be expressed for eth element in domain Ω_m^e as [57]

$$\mathbf{K}^e = \sum_{m=1}^{n_m}\int_{\Omega_m^e} \mathbf{B}_m^{\top}\bar{\mathbf{Q}}_m\mathbf{B}_m \,\mathrm{d}\Omega_m^e \tag{25}$$

The notations used in the above expression i.e. m, n_e, $\mathbf{B}_m$ and $\bar{\mathbf{Q}}_m$ denote the corresponding ply, number of elements, strain–displacement transfer matrix and transformed constituent matrix, respectively. The transformed constituent matrix is evaluated by $\bar{\mathbf{Q}}_m = \mathbf{T}_m^{\top}\mathbf{Q}_m\mathbf{T}_m$, where $\mathbf{T}_m$ represents the transformation using the direction cosines w.r.t. angle of the ply θ_c^m and the constituent matrix $\mathbf{Q}_m$ is determined using the material properties i.e. elastic moduli E_1^m, E_2^m, shear moduli $G_{12}^m, G_{13}^m, G_{23}^m$ and Poisson's ratio ν^m of the plate. Similarly using the kinetic energy equation, the element-wise mass matrix of the plate with density ρ_c^m can be expressed as

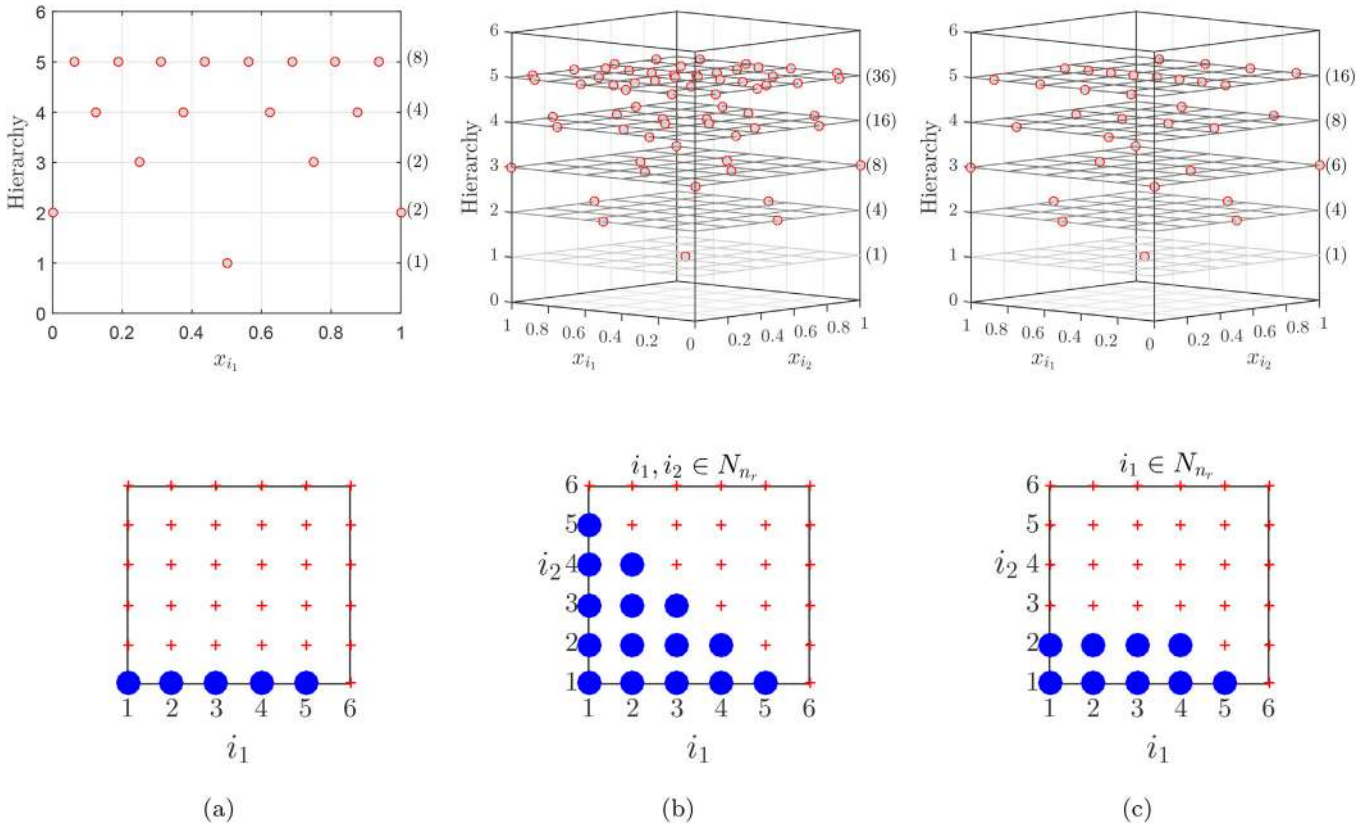

Fig. 2. Hierarchal generation of sparse grids for different cases with (a) one random variable, (b) two random variables and (c) two random variables but only one is significant (i.e. x_{i_1}), here the number of points from each hierarchy is given in the brackets.

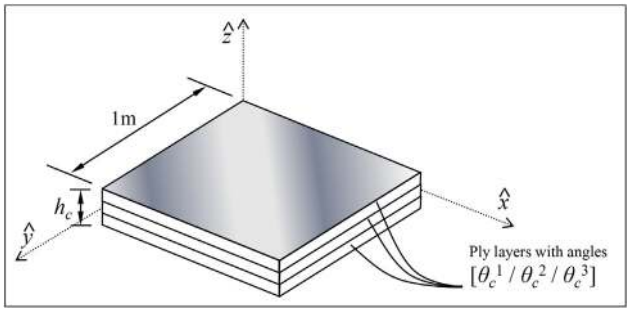

Fig. 3. A multi-layered laminated composite plate used in this study.

$$\mathbf{M}^e = \sum_{m=1}^{n_m} \int_{V_m^e} \mathbf{N}_m^{\mathsf{T}} \mathbf{P}_m \mathbf{N}_m \, \mathrm{d}V_m^e \tag{26}$$

where, $\mathbf{P}_m = \int_{-h/2}^{+h/2} \rho_c^m \, \mathrm{d}\hat{z}$, $\mathbf{N}_m$ is the shape function matrix and V represents the volume of the system.

In deterministic FE analysis, the material properties embedded in $\mathbf{M}_e$ and $\mathbf{K}_e$ matrices are set at fixed values. However, in the stochastic approach these properties are defined in a probability space $(\Theta, \mathcal{F}, \mathcal{P})$ which makes them function of $\theta \in \Theta$. To model this stochastic nature, random field approach is often adopted with the FE description discussed above. Karhunen-Loéve expansion (KLE) is considered here to express the random field $\mathcal{H}(\hat{\mathbf{x}}, \theta)$ in discrete quantities following a truncated spectral decomposition as given below [58]

$$\mathcal{H}(\hat{\mathbf{x}}, \theta) \approx \mu_{\mathcal{H}}(\hat{\mathbf{x}}) + \sum_{i=1}^{M} \sqrt{\lambda_i} z_i(\theta) \psi_i(\hat{\mathbf{x}}) \tag{27}$$

In the above equation, $\mu_{\mathcal{H}}(\hat{\mathbf{x}})$ and M represent the mean of the random field and the number of terms in the discretization. Moreover, λ_i and $\psi_i(\hat{\mathbf{x}})$ denote the solutions from an eigenvalue problem which are evaluated from the autocovariance function $C_{\mathcal{H}\mathcal{H}}[\hat{\mathbf{x}}, \hat{\mathbf{x}}'] = \mathbb{E}[\mathcal{H}(\hat{\mathbf{x}}, \theta)\mathcal{H}(\hat{\mathbf{x}}', \theta)]$. The kernels of this covariance function can be determined using various forms available in the literature [59]. In this study, exponential form is employed as expressed below [60]

$$C_{\mathcal{H}\mathcal{H}}[\hat{\mathbf{x}}, \hat{\mathbf{x}}'] = \sigma^2 . \rho(\hat{\mathbf{x}}, \hat{\mathbf{x}}') = \sigma^2 . \exp\left[-\left\{ \frac{|\hat{x} - \hat{x}'|}{l_{\hat{x}}} + \frac{|\hat{y} - \hat{y}'|}{l_{\hat{y}}} \right\} \right] \tag{28}$$

where, σ^2 is the variance of the homogeneous random field, $\hat{\mathbf{x}}, \hat{\mathbf{x}}'$ represent the spatial coordinates and the correlation lengths $l_{\hat{x}}, l_{\hat{y}}$ are along $\hat{x}$ and $\hat{y}$ axes, respectively. Here, the term homogeneous is associated with the randomness and is not related to the homogeneous material property. It may be noted that the value of these lengths influence the correlation in the discretized field such that $l_{\hat{x}}, l_{\hat{y}} \to \infty$ makes the correlation structure equal (i.e. random variable approach).

Let E_1^m and ρ_c^m follow Gaussian distribution using these properties in Eq. (27), the field can be expressed as

$$\begin{aligned} E_1^m(\hat{\mathbf{x}}, \theta) &= \mu_1^m + \sum_{i=1}^{M} \sqrt{\lambda_{mi}^{(1)}} z_{mi}^{(1)}(\theta) \psi_{mi}^{(1)}(\hat{\mathbf{x}}), \rho_c^m(\hat{\mathbf{x}}, \theta) \\ &= \mu_2^m + \sum_{i=1}^{M} \sqrt{\lambda_{mi}^{(2)}} z_{mi}^{(2)}(\theta) \psi_{mi}^{(2)}(\hat{\mathbf{x}}) \end{aligned} \tag{29}$$

Substituting Eq. (29) into Eqs. (25) and (26) result in

$$\mathbf{K}^e(\hat{\mathbf{x}}, \theta) = \sum_{m=1}^{n_m} \left[\mathbf{K}_m^{e0} + \sum_{i=1}^{M} \mathbf{K}_{mi}^{e1}(\hat{\mathbf{x}}) z_{mi}^{(1)}(\theta) \right] \tag{30}$$

and

$$\mathbf{M}^e(\hat{\mathbf{x}}, \theta) = \sum_{m=1}^{n_m} \left[\mathbf{M}_m^{e0} + \sum_{i=1}^{M} \mathbf{M}_{mi}^{e2}(\hat{\mathbf{x}}) z_{mi}^{(2)}(\theta) \right] \tag{31}$$

respectively. Here, the sub-matrices in Eqs. (30) and (31) are evaluated as $\mathbf{K}_m^{e0} = \int_{\Omega_m^e} \mu_1^m \mathbf{B}_m^{\mathrm{T}} \bar{\mathbf{Q}}_m \mathbf{B}_m \, \mathrm{d}\Omega_m^e$, $\mathbf{K}_{mi}^{e1}(\hat{\mathbf{x}}) = \int_{\Omega_m^e} \sqrt{\lambda_{mi}^{(1)}} \psi_{mi}^{(1)}(\hat{\mathbf{x}}) \mathbf{B}_m^{\mathrm{T}} \bar{\mathbf{Q}}_m \mathbf{B}_m \, \mathrm{d}\Omega_m^e$, $\mathbf{M}_m^{e0} = \int_{V_m^e} \mu_2^m \mathbf{N}_m^{\mathrm{T}} \mathbf{P}_m \mathbf{N}_m \, \mathrm{d}V_m^e$ and $\mathbf{M}_{mi}^{e2}(\hat{\mathbf{x}}) = \int_{V_m^e} \sqrt{\lambda_{mi}^{(2)}} \psi_{mi}^{(2)}(\hat{\mathbf{x}}) \ \mathbf{N}_m^{\mathrm{T}} \mathbf{P}_m \mathbf{N}_m \, \mathrm{d}V_m^e$. Using these element matrices, the global stiffness and mass matrices i.e. $\mathbf{K}(\hat{\mathbf{x}}, \theta)$ and $\mathbf{M}(\hat{\mathbf{x}}, \theta)$ are determined as suggested by Chen and Soares [61]. Incorporating this stochastic formulation in static analysis, the governing equation takes the following form

$$\left[\sum_{m=1}^{n_m} \mathbf{K}_m^0 + \sum_{j=1}^{n_m M} \mathbf{K}_j^1(\hat{\mathbf{x}}) z_j^{(1)}(\theta) \right] \mathbf{u}(\theta) = \mathbf{f} \tag{32}$$

On solving Eq. (32), stresses $\boldsymbol{\sigma}(\hat{\mathbf{x}}, \theta) = \{\sigma_1(\hat{\mathbf{x}}, \theta) \ \sigma_2(\hat{\mathbf{x}}, \theta) \ \tau_{12}(\hat{\mathbf{x}}, \theta)\}^{\mathrm{T}}$ at Gauss quadrature points are determined in the ply using $\bar{\mathbf{Q}}_m(\hat{\mathbf{x}}, \theta)$. In the present study, failure index $\mathfrak{F}$ is adopted to quantify the performance of the composite plate under static loading using modified Tsai-Hill failure criterion [60]

$$\mathfrak{F}(\hat{\mathbf{x}}, \theta) = \left(\frac{\sigma_1(\hat{\mathbf{x}}, \theta)}{X} \right)^2 + \left(\frac{\sigma_2(\hat{\mathbf{x}}, \theta)}{Y} \right)^2 + \left(\frac{\tau_{12}(\hat{\mathbf{x}}, \theta)}{S} \right)^2 - \frac{\sigma_1(\hat{\mathbf{x}}, \theta) \sigma_2(\hat{\mathbf{x}}, \theta)}{X^2} \tag{33}$$

This criterion incorporates the longitudinal, transverse and shear strengths (i.e. X, Y and S, respectively) of the composite plate where $\mathfrak{F}(\hat{\mathbf{x}}, \theta) \geqslant 1$ corresponds to failure. Similarly, the formulation can be extended for the dynamics analysis where the Lagrange equation can be invoked to get the dynamic equilibrium in the following form

$$\begin{aligned} &\left[\sum_{m=1}^{n_m} \mathbf{M}_m^0 + \sum_{j=1}^{n_m M} \mathbf{M}_j^2(\hat{\mathbf{x}}) z_j^{(2)}(\theta) \right] \ddot{\mathbf{u}}(\theta, t) \\ &+ \left[\sum_{m=1}^{n_m} \mathbf{K}_m^0 + \sum_{j=1}^{n_m M} \mathbf{K}_j^1(\hat{\mathbf{x}}) z_j^{(1)}(\theta) \right] \mathbf{u}(\theta, t) \\ &= \mathbf{f}(t) \end{aligned} \tag{34}$$

For free vibration, it can be solved as an eigenvalue problem which is given by

$$\begin{aligned} &\left[\sum_{m=1}^{n_m} \mathbf{K}_m^0 + \sum_{j=1}^{n_m M} \mathbf{K}_j^1(\hat{\mathbf{x}}) z_j^{(1)}(\theta) \right]^{-1} \left[\sum_{m=1}^{n_m} \mathbf{M}_m^0 + \sum_{j=1}^{n_m M} \mathbf{M}_j^2(\hat{\mathbf{x}}) z_j^{(2)}(\theta) \right] \mathbf{u}(\theta, t) \\ &= \frac{1}{\{n_f(\theta)\}^2} \mathbf{u}(\theta, t) \end{aligned} \tag{35}$$

where, n_f is the natural frequency of the composite plate. The uncertainty propagating due to θ can be quantified using the proposed approach as discussed in the next section.

4. Application in stochastic computation

In this section, the proposed *hd*A-HDMR is discussed for different applications in the stochastic field. As the method employs an iterative framework based on the adaptive contributions of the multiple HDMRs, it requires adequate selection of the component surfaces. In this regard, selection of the reference point(s) after the initial iteration is a critical task to achieve the desired objective. Hence, as a solution to this issue, the objective of the problem is defined to determine the region of interest which can be either the optimal locations like MPP, maxima/minima or the favourable locations in a probabilistic sense depending upon the problem statement are as follows:

- **Uncertainty Quantification:** In uncertainty analysis, the response surface is required to map the statistically favourable regions, like area near mean, tail ends etc., accurately to estimate the moments. Hence, the components of HDMR and support points are required to be generated in these regions of interest. In this regard, without the loss of generality, the reference point is preferably selected at the mean values of the random variables in the first iteration. The support points are generated following their respective probability distributions. This can be performed by mapping the CDF as

$$\mathbf{x} = F_{\mathbf{X}}^{-1}[\Phi(\mathbf{z})] \tag{36}$$

if the random variables are uncorrelated. In the above expression, notations $F_{\mathbf{X}}(\bullet)$ and $\Phi(\bullet)$ represent the CDFs of $\mathbf{x}$ and $\mathbf{z}$, respectively. Apart from the distribution based influence, multiple generations of the support points in iterative manner is performed by assuming same reference location such that $\mathbf{c}^{it} = \mathbf{c}^{it-1}$. However, the influence domain of the support point is reduced using the reduction factor $\lambda_{\mathbf{x}}$. This factor iteratively reduces the extent of $\Omega_{\mathbf{x}}$ in successive generations unless otherwise mentioned for the specific case. In this study, the reduction factor is assumed to be 0.75 for the uncertainty quantification. Once the global *hd*A-HDMR is constructed, population based sampling schemes (e.g. MCS) with adequate sample size is adopted for the uncertainty quantification.
- **Reliability Analysis:** The region of interest in the reliability analysis is the limit state (i.e. $g(\mathbf{x}) = 0$), especially near the failure point or MPP. Hence, in this study, a MPP based optimization is demonstrated using *hd*A-HDMR to determine the probability of failure. As explained earlier, the use of Hermite polynomials makes the optimization straightforward for this analysis which takes the following form

$$\begin{aligned} &\text{Minimize} && \sqrt{\mathbf{z}\mathbf{z}^{\mathrm{T}}} \text{ w.r.t. } \mathbf{z} \\ &\text{Subjected to :} && \tilde{g}(\mathbf{x}) \leqslant 0 \\ & && \mathbf{x} \in \Omega_{\mathbf{x}} \end{aligned} \tag{37}$$

The solution of the above optimization process gives the MPP as $\mathbf{z}^{*,it}$ and subsequently, $\mathbf{x}^{*,it}$ for that iteration which is followed by successive iterations to locate the actual MPP for the problem. Hence, additional points are added in these successive iterations to improve the quality of *hd*A-HDMR. These additional points are generated around the MPP evaluated in each iteration i.e. $\mathbf{c}^{(it+1)} = \mathbf{x}^{*,it}$. The convergence of this process is checked using permissible errors $\mathcal{E}_1$ and $\mathcal{E}_2$ for the change in the $\tilde{g}(\mathbf{x}^{*,\bullet})$ and $\mathbf{z}^{*,\bullet}$. Usually, the values of these permissible errors ranges within 10^{-2}–10^{-3}. Once the global surface is ready, simulation techniques are adopted for failure estimation.
- **Reliability Based Design Optimization:** RBDO problem solves a constraint optimization to determine the design point $\mathbf{x}_d^{*,it}$ in the variable space $\Omega_{\mathbf{x}_d}$ which is given by

$$\begin{aligned} &\text{Maximize} && \mathbf{x}_d \\ &\text{Subjected to :} && \mathcal{P}[\tilde{g}(\mathbf{x}, \mathbf{x}_d) \leqslant 0] = p_f^* \\ & && \mathbf{x}_d \in \Omega_{\mathbf{x}_d} \end{aligned} \tag{38}$$

where, $\mathcal{P}[\bullet]$ denotes the probability of occurrences defined in $[\bullet]$ and $\mathbf{x}_d$ is the design variable vector which can be random or deterministic in nature. To solve the above equation, response surface is built using both $\mathbf{x}$ and $\mathbf{x}_d$. The new reference points are defined using the optimized value of $\mathbf{x}_d$ and the mean values of $\mathbf{x}$ when the iterations are continued till the convergence is achieved satisfactorily. In this regard, permissible tolerance for the convergence of the $\mathbf{x}_d^{*,\bullet}$ is chosen as discussed in the reliability analysis (i.e. $\mathcal{E}_1$ and $\mathcal{E}_2$).

Above applications bypass multiple evaluations of the original stochastic FE model required in the simulation and ease the computational burden. It can be noted that the nonlinear multidimensional optimization processes as in Eqs. (37) and (38) can be solved using any standard tool available in the literature [62]. The present study employs SQP technique available in the MATLAB® [63]. A flowchart summarizing the complete process for different applications is presented in Fig. 4. Following these steps, the numerical simulations are

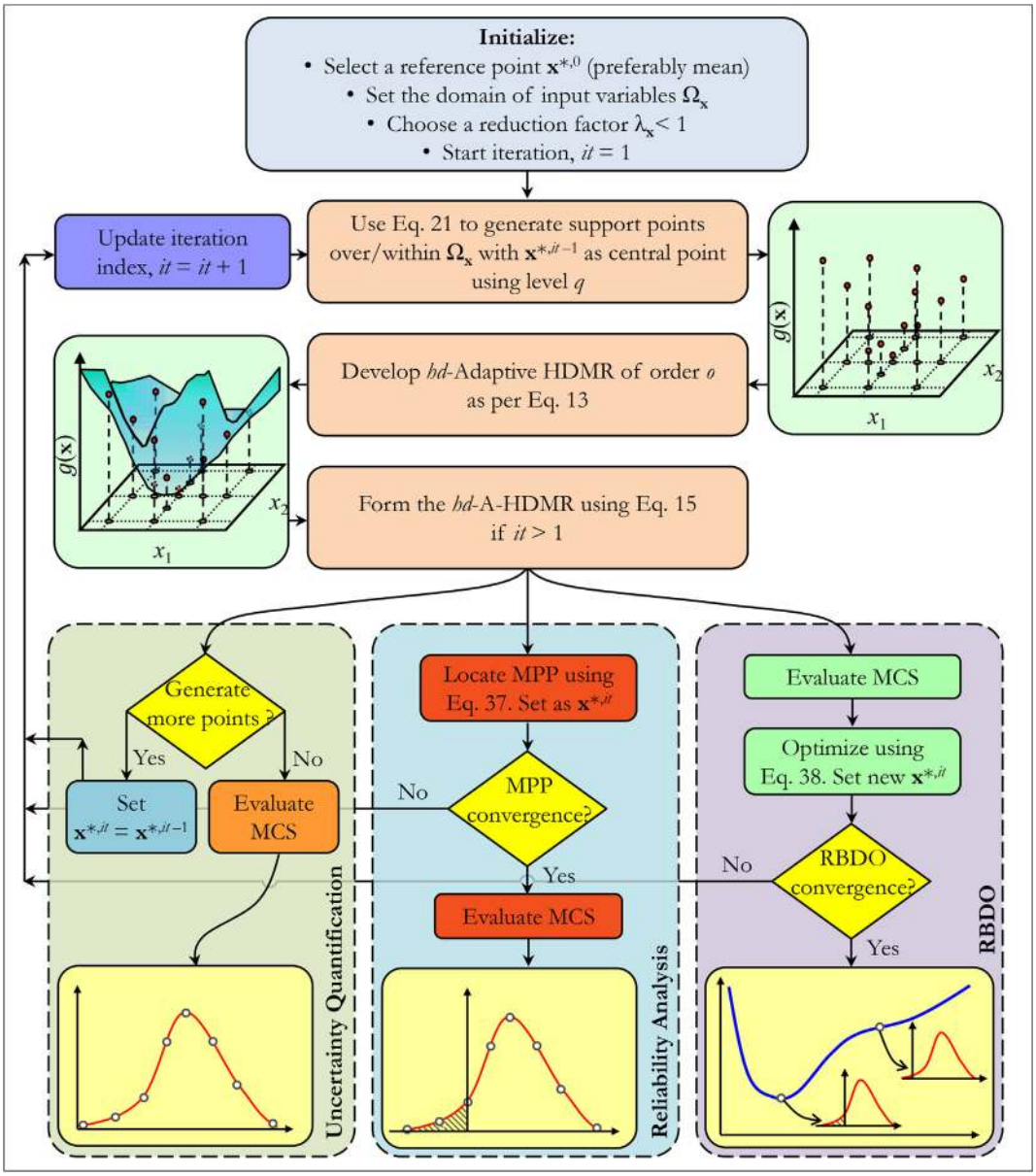

Fig. 4. Flowchart of the proposed algorithms using *hd*AMFD-HDMR for uncertainty quantification, reliability analysis and RBDO.

performed to justify the merits of the proposed hybrid *d*-Adaptive HDMR in the upcoming section.

5. Results and discussion

In this section, the proposed *hd*A-HDMR is implemented for stochastic FE analysis of composite plates to determine the free vibration characteristic and failure index when subjected to transverse loading. The performance function $g(\mathbf{x})$ for stochastic computation includes the limit states based on the failure index (i.e. $1 - \mathfrak{F}$) and natural frequencies n_f. It is dependent on the random fields and variables $\mathbf{x}$ as specified at respective locations within the section. The composite plate is characterised by the two-dimensional homogeneous random field for the material properties that are modeled using KLE. The standard input variable $\mathbf{z}$ following standard normal distribution is considered based on its wider acceptance. The proposed method is used here for uncertainty quantification, reliability analysis and design optimization. The problem is solved using other similar methods like MLS-HDMR [34,22,35], RS-HDMR [27] and Kriging [64] for comparison. The MLS-HDMR [22,34,35] is a finite difference HDMR where the component functions are modeled by regular polynomial bases. It is formed using cartesian grid based support points with coordinates $c_i - (k-j)\sigma_{x_i}, c_i$ and $c_i + (k-j)\sigma_{x_i}$, where σ_{x_i} represents the standard deviation of ith variable, k is the level of support points and index $j = 1, 2, \ldots, k-1$. The coordinates of the reference point c_i are set at the mean μ_{x_i} of the random variables and the number of support points for order o is evaluated using $n_s = \sum_{i=0}^{o} \frac{n!(n_a-1)^i}{(n-i)!i!}$ with $n_a = 2k-1$. MLS technique is utilized to determine the coefficients associated with the regular polynomial bases i.e. $\left[1\ x_1\ x_2\ \ldots\ x_n\ x_1^2\ x_1x_2\ \ldots\ x_n^2\right]$ in the component functions. The weight function employed as suggested in Chowdhury et al. [22,34,35] to assist the MLS based calculations. RS-HDMR [27] involves quasi random sampling like Sobol' sequence to represent the component functions based on the orthogonal polynomials like modified Legendre polynomial as given by Dey et al. [28]. The degree of these polynomials are adaptive based on the Sobol' sensitivity index. Both these methods employ a single generation of the

HDMR to construct the dimension decomposition based response surface. The third method considered in this study is Kriging using DACE Toolbox [64] which also uses regular polynomial bases. In addition to the bases, weight functions are defined between the support points to form the meta-model. It uses a random sampling scheme such as LHS to generate the support points. The efficacy of these methods are justified based on the computational effort involved in the simulation and the accuracy of the results. In this study, the accuracy of the aforementioned methods is determined using MCS with adequate sample size as the benchmark. The computational cost is indicated based on the number of original FE analysis performed. This indicates the amount of CPU time consumed by the particular method for computation. The inference from the numerical analysis is presented in the following subsections.

5.1. Uncertainty quantification

A square cantilever composite laminated plate is modeled here which is made of graphite-epoxy stacked in different angles. The stacking sequence of these plies are considered as random with mean at $[-45/+45/-45]$ (in degree) having 10% coefficient of variation (cov). The deterministic values of the material properties are as follows: $E_2 = 8.90$ GPa, $G_{12} = 7.10$ GPa, $G_{23} = 2.84$ GPa and $G_{13} = 7.10$ GPa [28]. The other material properties of the graphite-epoxy composite plate such as E_1 and ρ_c are considered as two-directional independent homogeneous Gaussian random fields with mean at 138.00 GPa and 3202.00 kg/m^3, respectively, where Poisson's ratio $\nu \sim \mathcal{N}(0.3000, 0.0009)$. The standard deviation $\sigma_{\mathbf{x}}$ of these fields are defined as 13.80 GPa and 320.20 kg/m^3, and the correlation lengths $l_{\hat{x}}, l_{\hat{y}}$ as 0.50. Using these statistical properties, the covariance function of the random fields are given by $\sigma_{\mathbf{x}}\rho(\hat{\mathbf{x}}, \hat{\mathbf{x}}')$. The thickness of the laminas are equal and the thickness to length ratio (i.e. h_c/b) of the composite plate is 0.004. Stochastic FE analysis is performed using a 6×6 mesh with uniform size. Each element of the plate is modeled using nine-noded quadrilateral isoparametric elements, hence a total of 155 nodes are formed in the FE model. The fields are discretized to form the vectors of random fields with respect to 36 elements using KLE as described in Section 3.

In this study, free vibration analysis is carried out to determine the first five natural frequencies of the composite plate. These frequencies and the corresponding mode shapes are obtained using the above mentioned properties. Direct MCS is adopted to determine the frequencies using 10^4 realizations. The effect of uncertainties on the modal properties are presented in Fig. 5. The probability distribution functions of these modal parameters obtained from MCS are plotted in Fig. 6 which are considered as the benchmark for further analysis. Apart from MCS, other meta-models are also used to quantify the uncertainties in the natural frequencies. It can be seen in Fig. 6 that the *pdf*s obtained from RS-HDMR have significant mismatch with MCS. This is due to the unwanted effects of the spurious component functions. The number of FE solutions carried out to construct this model is 3000 with 2$^{\text{nd}}$ order component functions. The lower and upper bounds of the support points are set to $\mu_{\mathbf{x}} \pm h_r\sigma_{\mathbf{x}}$, where $h_r = 1$. The maximum degree of the orthogonal polynomial basis is fixed at 5. MLS based finite difference-HDMR is then employed which improves the results from the previous case i.e. RS-HDMR. However, it still yields significant error, especially for first four natural frequencies as shown in Fig. 6(a)–(d). In this case, the order o of the HDMR is reduced to 1 as the number of support points required to form the 2nd response surface is high (> 3000). A total of 609 FE evaluations are used for the level of grid points $k = 4$. The results explain that even if it considers till the 1st order terms (i.e. no combined effects are used), the accuracy is inconsistent. Hence, the performance of the above two methods infer that an adaptive selection of the order should provide the desired results. However, before using the proposed algorithm, performance of the Kriging based meta-model is also verified in this study to quantify the uncertainties. Support points are generated using LHS with a sample size of 3000 to construct this meta-model. The 4th and 5th natural frequencies observe a close match with the MCS results, however, the first three natural frequencies face error in estimation. Finally, the proposed *hd*A-HDMR is used which shows a close match with the MCS results and distinctly marks its accuracy with respect to other methods applied here. This dimension decomposition is built in two iterations

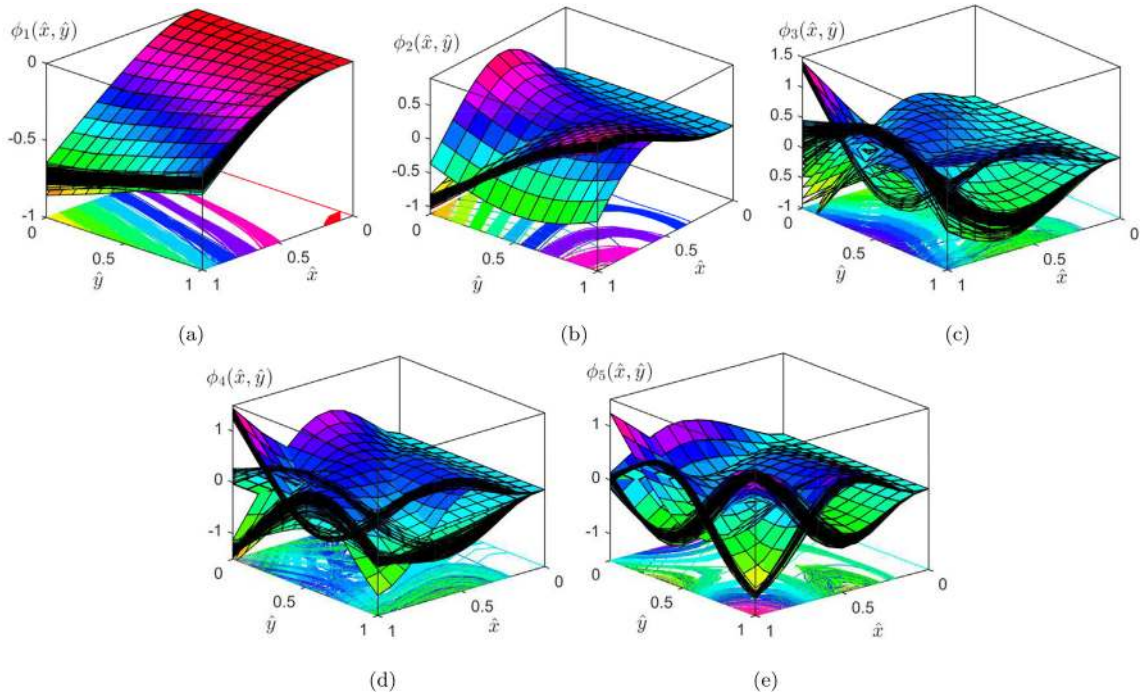

Fig. 5. Mode shapes due to stochastic material properties where (a) mode 1, (b) mode 2, (c) mode 3, (d) mode 4 and (e) mode 5.

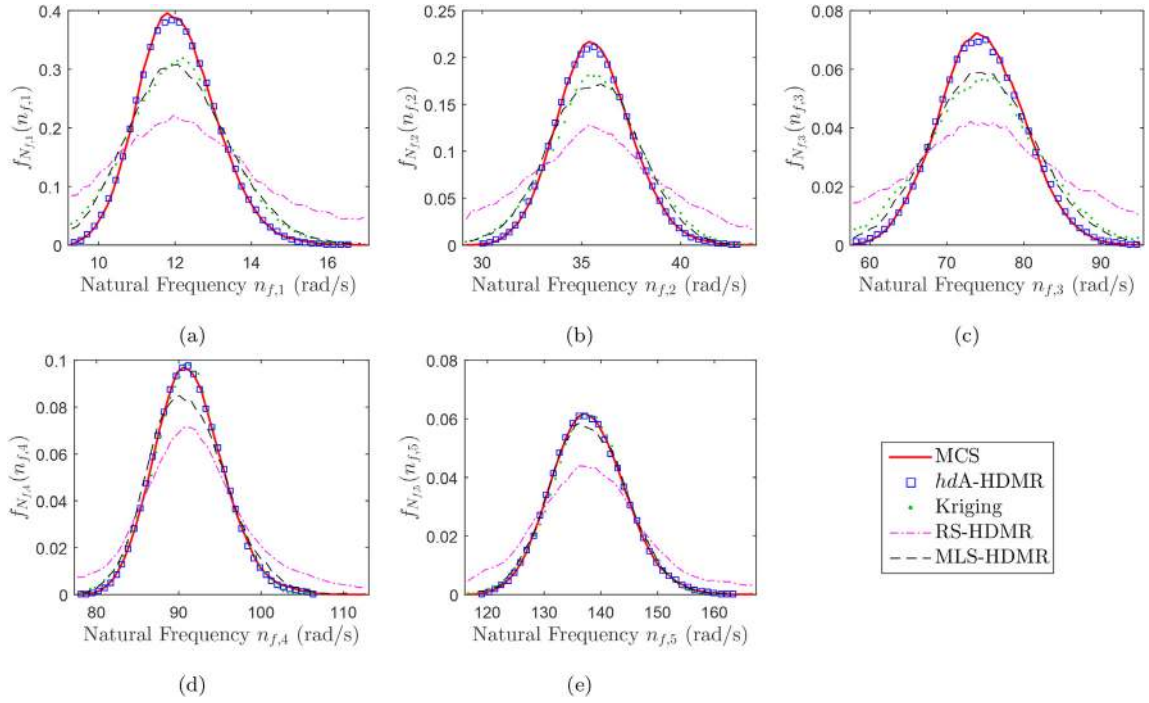

Fig. 6. Comparison of *pdf* of modal responses from a spatially uncertain cantilever composite plate where (a) first, (b) second, (c) third, (d) fourth and (e) fifth natural frequencies.

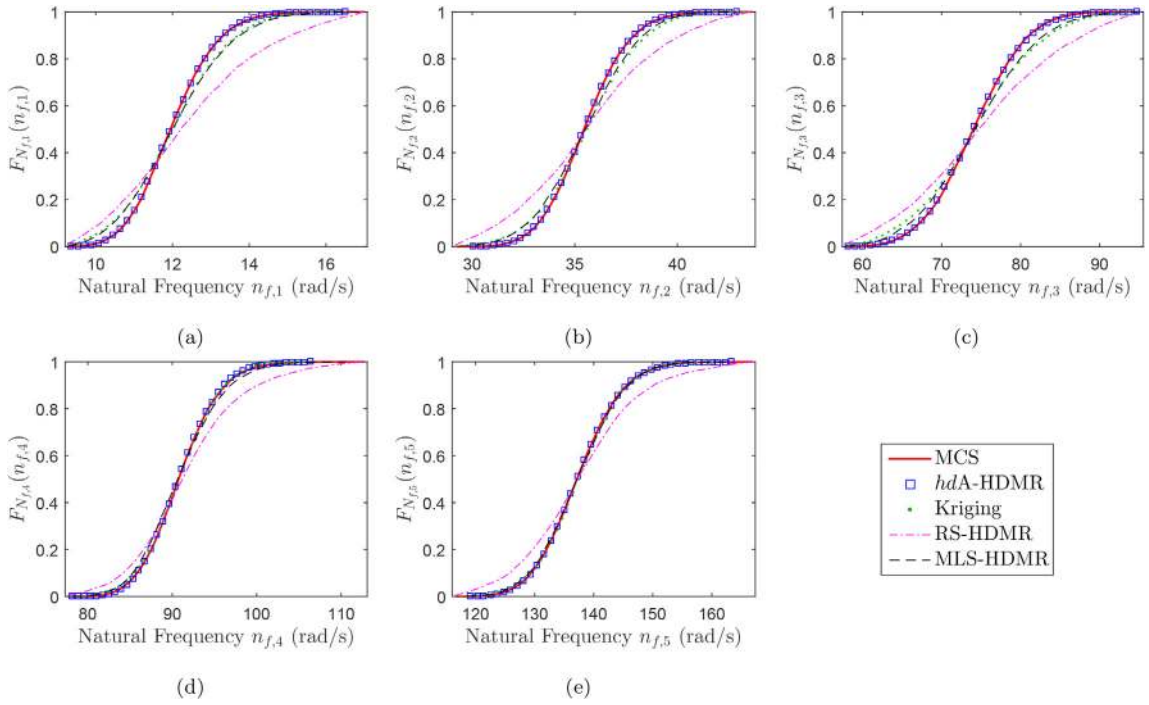

Fig. 7. Comparison of CDF of modal responses from a spatially uncertain cantilever composite plate where (a) first, (b) second, (c) third, (d) fourth and (e) fifth natural frequencies.

with first iteration starting at mean $\mu_{\mathbf{x}}$ as the reference point (i.e. $\mathbf{c}^{*,0}$). In this uncertainty quantification, no objective function is defined, hence the second iteration follow the same reference point but the bounds of the support points are reduced by 25% prior to populate with more points. Overall, the proposed method offers a better fit and can map the *pdf*s of the first five natural frequencies with an insignificant error of estimation.

The CDF of the natural frequencies are also plotted in Fig. 7a which shows the accuracy of different methods when compared with the MCS data. A comparative study is performed based on the statistical moments (such as mean, standard deviation, skewness and kurtosis) of the first five fundamental frequencies as shown in Table 1. The tabulated results show adequate match in the estimation of the first moment (i.e. mean) among all the methods performed in this study

Table 1
Statistical properties of the first five stochastic natural frequencies of a cantilever composite plate (units in rad/s).

Nat. Freq.	Method	Mean	Std. Dev.	Skewness	Kurtosis
	Direct MCS	12.090	1.001	0.388	3.325
	*hd*A-HDMR	12.085	0.998	0.318	3.137
1	Kriging	12.063	1.318	0.008	3.060
	MLS-HDMR	12.117	1.309	0.244	3.076
	RS-HDMR	10.712	36.167	−2.735	79.482
	Direct MCS	35.658	1.828	0.213	3.119
	*hd*A-HDMR	35.639	1.837	0.193	3.091
2	Kriging	35.761	2.257	−0.022	3.001
	MLS-HDMR	35.635	2.215	−0.039	2.965
	RS-HDMR	33.854	60.939	−3.267	100.820
	Direct MCS	74.504	5.366	0.096	2.878
	*hd*A-HDMR	74.508	5.500	0.109	3.078
3	Kriging	74.544	7.306	0.014	3.039
	MLS-HDMR	74.710	6.710	0.094	2.986
	RS-HDMR	68.492	181.320	−5.270	120.810
	Direct MCS	91.317	4.113	0.366	3.385
	*hd*A-HDMR	91.240	4.034	0.283	3.161
4	Kriging	91.099	4.150	−0.005	3.000
	MLS-HDMR	91.255	4.591	0.351	3.179
	RS-HDMR	90.467	118.290	−2.380	112.870
	Direct MCS	137.900	6.361	0.244	3.171
	*hd*A-HDMR	137.860	6.333	0.250	3.123
5	Kriging	137.900	6.471	−0.011	3.013
	MLS-HDMR	137.780	6.592	0.100	3.001
	RS-HDMR	137.570	134.220	−2.427	93.551

Note: The number of FE calls by MCS, *hd*A-HDMR, Kriging, MLS-HDMR and RS-HDMR are 10^4, 730, 3000, 609 and 3000, respectively.

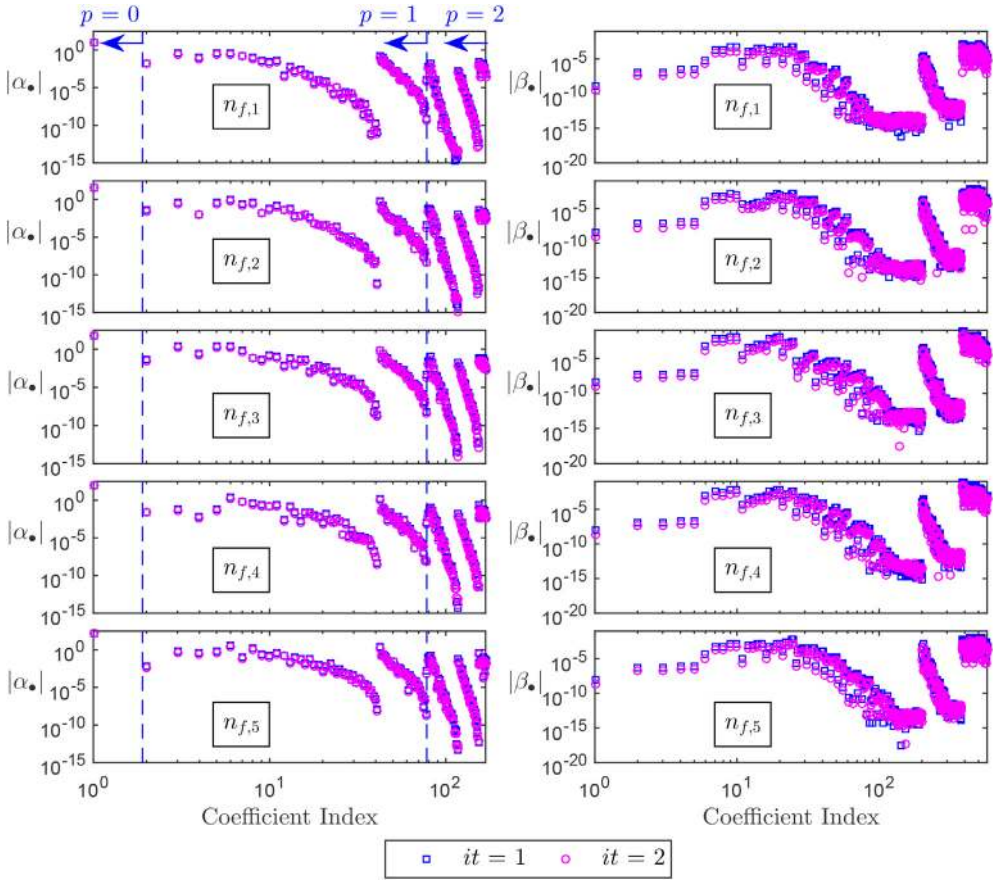

Fig. 8. Magnitude of the unknown coefficients (i.e., $\alpha_\bullet$ and $\beta_\bullet$) associated with PCE and nonparametric terms, respectively, evaluated to determine the natural frequencies of a cantilever composite plate. For $\alpha_\bullet$, the coefficient indices to the left of the vertical dashed lines correspond terms not larger than the specified degree p of PCE.

except RS-HDMR. Higher moments show better quality when the proposed *hd*A-HDMR is used as compared to the other methods. This proves the consistency of the proposed method as compared to the other models adopted here. As a general observation among all these methods, the performance of the RS-HDMR is significantly erroneous for stochastic finite element analysis. In this context, a dimension adaptive version of the multiple finite difference-HDMR has proved to be accurate for stochastic computations. The unknown coefficients obtained from *hd*A-HDMR for these natural frequencies n_f are presented in Fig. 8a. As mentioned, both the iterations (i.e. $it = 1$ and 2) are plotted and the coefficients are depicted using a numbered index sequence following ν, θ_c, ρ_c and E_1 as 1, 2–4, 5–40 and 41–76, respectively. The polynomial based coefficient $\alpha_\bullet$ is segregated as per degree p. It observes sudden change in the magnitude which is attributed to the two random fields ρ_c and E_1 in this illustration. These fields start from the coefficient index 6 to 41 and 42 to 77, respectively, for $p = 1$ and same trend can be observed for degree $p = 2$. This truncated PCE is assisted by nonparametric terms corresponding to error modeling coefficient $\beta_\bullet$ which is indexed in the same sequence. However, unlike $\alpha_\bullet$, it is not dependent on p and hence, its numbering is based on the occurrence in the full expansion. The coefficient $\beta_\bullet$ also reflects the acute change in the magnitude due to the indexing of the random fields.

The proposed *hd*A-HDMR is also adopted to solve for a simply supported composite plate with non-normal random fields subjected to UDL. The dimensions for this plate remains unaltered with thickness $h = 0.010$ m where the thickness of each angel ply is equal and the angle stacking sequence is [0/90/0] (in degree). In this example, three non-normal random fields and six random variables are considered which are related to strength of the plate. The elastic moduli $E_1(\hat{x},\hat{y}) = F_{E_1}^{-1}[\Phi_{Z_1}(z_1(\hat{x},\hat{y}))]$ and $E_2(\hat{x},\hat{y}) = F_{E_2}^{-1}[\Phi_{Z_2}(z_2(\hat{x},\hat{y}))]$ are defined as random fields which follow two-dimensional homogenous and independent Weibull distribution $\mathcal{W}(a_\mathcal{W}, b_\mathcal{W})$ i.e.

$$f_X(x|a_\mathcal{W}, b_\mathcal{W}) = \frac{b_\mathcal{W}}{a_\mathcal{W}}\left(\frac{x}{a_\mathcal{W}}\right)^{b_\mathcal{W}-1}\exp\left[-\left(\frac{x}{a_\mathcal{W}}\right)^{b_\mathcal{W}}\right] \quad \forall x \geqslant 0 \tag{39}$$

The distribution in the above equation is defined for the realization x at $(\hat{x}_i,\hat{y}_j)$ with $a_\mathcal{W}$ and $b_\mathcal{W}$ representing its scale and shape parameters, respectively. These parameters are given as $E_1 \sim \mathcal{W}(158.90, 20.70)$ and $E_2 \sim \mathcal{W}(9.00, 14.40)$ for the aforementioned random fields as suggested by Sasikumar et al. [60]. Here, the notation Z_i denotes Gaussian random field with mean 154.900 GPa, 8.700 GPa and cov 5.90%, 9.50% for $i = 1, 2$, respectively. The third random field is defined for shear modulus $G_{12}(\hat{x},\hat{y}) = c_3\exp[\alpha_3(\hat{x},\hat{y})]$ which is modeled using log-normal distribution with mean 4.500 GPa and cov 8.80%. The parameters in this random field are evaluated as $c_3 = \mu_{x_3}^2/\sqrt{\mu_{x_3}^2+\sigma_{x_3}^2} = \mu_{x_3}/\sqrt{1+\mathrm{cov}_3}$ and $\alpha_3(\hat{x},\hat{y})$ represents a Gaussian random field with mean zero and covariance function equal to $\ln\left(1+\mathrm{cov}_{x_3}^2\right).\rho(\hat{\mathbf{x}},\hat{\mathbf{x}}')$. The correlation structures are considered as isoparametric for this example with values of the correlation lengths fixed at 0.40 [36,60]. The other properties i.e. ν, X_t, X_c, Y_t, Y_c and S as considered as random variables such that $l_{\hat{x}}, l_{\hat{y}} \to \infty$. Among these, ν, X_t, X_c, S follow lognormal distribution with mean 0.281, 2.409 GPa, 1.148 GPa, 0.083 GPa and cov (in %) 7.50, 6.70, 18.10, 5.00 whereas Y_t, Y_c (in MPa) are Weibull distributed with $\mathcal{W}(50.30, 5.80), \mathcal{W}(208.60, 7.40)$, respectively [36,60]. The subscripts in the properties i.e. $\bullet_t$ and $\bullet_c$ denote the strengths with respect to tension and compression. The composite plate is subjected to a two-dimensional uniformly distributed loading (i.e. along $\hat{x}$ and $\hat{y}$) of 73.558 kN/m^2. This load is determined corresponding to $\bar{\aleph} = 0.75$ as suggested by Sasikumar et al. [60]. The stochastic FE analysis is performed using a 6×6 uniform discretization of the random fields. Overall, the problem results in 114 (i.e. $6\times6\times3+6$) random variables with non-normal distributions. Fig. 9a shows the probability distribution of the failure index for this composite plate using MCS, *hd*A-HDMR, RS-HDMR, MLS-HDMR and Kriging. In this analysis, RS-HDMR, MLS-HDMR and Kriging call 3000, 685 and 3000 original function evaluations, respectively. The proposed *hd*A-HDMR requires 1380 function evaluations as opposed to 2067 (refer [36]) FE calls in *d*AMFD-HDMR. Fig. 9a demonstrates the accuracy in the *pdf* and CDF estimation of failure index obtained from different methods. These results show a close match between the probability distributions using the *hd*A-HDMR and MCS. MLS-HDMR with 1st order also offers better result among the other methods illustrated here. However, the level of accuracies obtained from the proposed method is superior to the others.

Another case study is performed for a non-rectangular simply supported composite plate using asymmetric ply orientation. A parallelogram shaped composite plate is adopted of length, slanted breadth and angle as 1 m, 1.2 m and 56.44°. The composite is made of carbon epoxy material M55J/M18 [60] where the properties, namely, ν, X_t (MPa), X_c (MPa), Y_t (MPa), Y_c (MPa) and S (MPa) follow $\mathcal{G}(1170.75, 0.00027)$, $\mathcal{W}(1981.83, 10.20)$, $\mathcal{W}(600.43, 24.00)$, $\mathcal{W}(21.58, 20.27), \mathcal{W}(106.96, 60.61)$ and $\mathcal{U}(52.48, 55.06)$, respectively. The nomenclature of the distributions and associated statistical parameters denote Gamma $\mathcal{G}$(shape, scale), Weibull $\mathcal{W}$(scale, shape), Lognormal $\mathcal{LN}$(mean, standard deviation) and Uniform $\mathcal{U}$(lower bound, upper bound) distributions. The remaining properties such as E_1 (GPa), E_2 (GPa) and G_{12} (GPa) are random fields following $\mathcal{W}(355.04, 19.26), \mathcal{U}(6.21, 6.93)$ and $\mathcal{LN}(1.519, 0.032)$, respectively. The correlation lengths are assumed as 1.00 and the field is uniformly discretized in 6×6 mesh pattern. The ply orientation is considered to

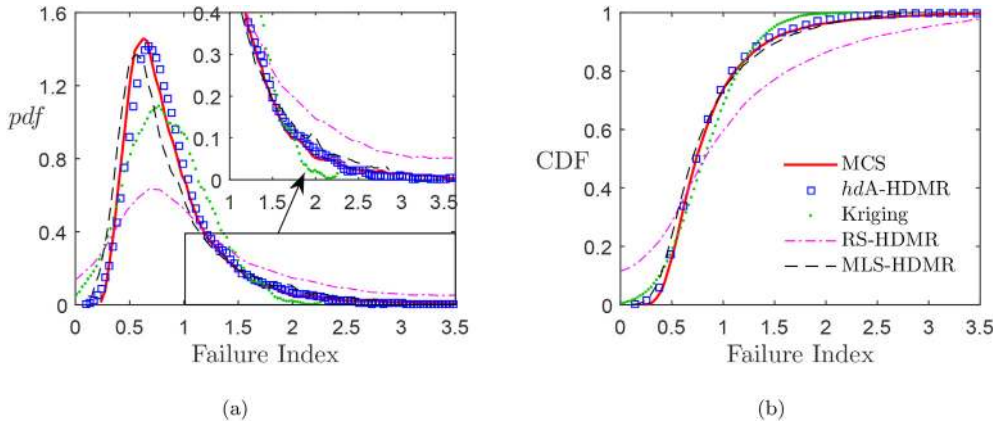

Fig. 9. Comparison of (a) *pdf* and (b) CDF based on failure index from a spatially uncertain simply supported composite plate using different methods.

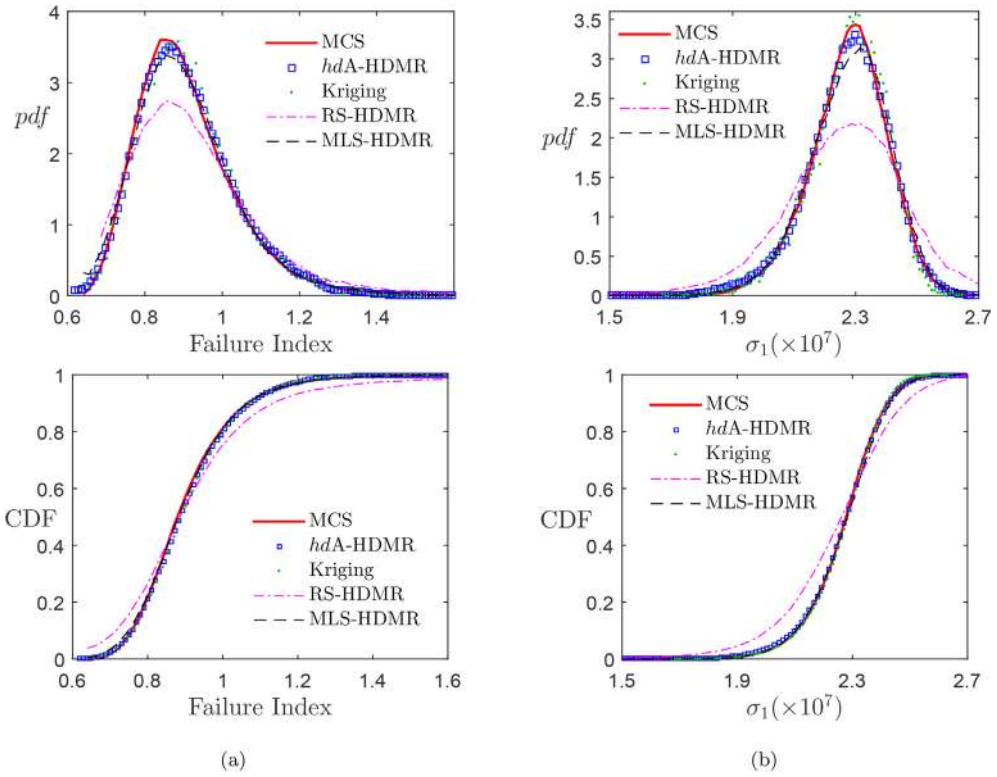

Fig. 10. Comparison of *pdf* and CDF based on (a) failure index and (b) σ_1 (N/m^2) of a spatially uncertain simply supported parallelogram shaped composite plate using different methods.

be [0/30/60] (in degree) and the plate is subjected to UDL of 18 kN/m^2. The uncertainty propagation in the failure index $\mathfrak{F}$ as expressed by Eq. (33) is estimated using different methods. It can be observed from Fig. 10a that Kriging, MLS-HDMR and RS-HDMR improves the prediction quality from the previous cases. However, they still yield notable mismatch in the *pdf* which is better mapped by the proposed method. Similar observations can be derived for the stress component σ_1 as depicted in Fig. 10a. Also, the unknown coefficients evaluated from *hd*A-HDMR are plotted in Fig. 11, where the variables are indexed in the order – $\nu, E_1, E_2, G_{12}, X_t, X_c, Y_t, Y_c$ and S positioned at 1, 2–37, 38–73, 74–109, 110, 111, 112, 113 and 114, respectively. The results illustrate similar observations as discussed above in the case of cantilever plate.

5.2. Reliability analysis

Using the aforementioned simply supported rectangular composite plate, probability of failure is estimated for different values of UDL to develop the fragility curve as shown in Fig. 12. For reliability analysis, a larger sample size of MCS (i.e. n_c = 5E5) is employed to estimate low p_f. The FE solutions made by different methods (i.e. RS-HDMR, MLS-HDMR and Kriging) for each load case remain same as mentioned in the above discussion. It is observed that the Kriging using DACE Toolbox [64] faces difficulty to deal with large dimensions. The issue is severe in the case of p_f estimation, especially for low p_f where sample size is inevitably large. The simulation technique adopted by the models require estimation of the weight between the support points and the sampled realizations as per Eq. (18). In this case, both these values (i.e. number of support points n_s and sample size n_c) are relatively high, hence it faces difficulty to compute the weight matrix **R** of the Gaussian process. Also, these calculations are performed simultaneously for all the coordinates of the support points as opposed to the MLS technique which employs a scalar approach where these calculations are performed one-by-one. This computational issue makes the application of Kriging based meta-model very slow and eventually, time exhaustive. The aforementioned issue is addressed in this study by the proposed hybrid *d*-Adaptive HDMR formulation which breaks the complete polynomial basis into smaller sub-matrices. It reduces the computational burden associated with the simultaneous calculations of the support points by dividing it into various sub-matrices. Also, it can be noted that deterministic sampling offered by the sparse grid scheme helps to reduce the computational cost associated with the calculation of weigh structure. This can be explained for any component function where only limited number of variables are effective due to dimension decomposition. Accordingly, these effective locations of the random variables are only considered for the weight function calculations. However, this is not the case for random sampling based DoE where irrespective of the component functions, all coordinates are considered. This problem makes Kriging [64] with random sampling less preferable for reliability analysis as all the variables need to be considered for weight function calculation. In brief, it can be stated that this process is streamlined in the present proposal which helps to improve efficiency. It ultimately yields at a much faster computation of the reliability analysis. In addition to this computational efficiency, the proposed method converges using 922 to 2067 support points for different load cases in the fragility curve. Fig. 12 shows the p_f estimated from this numerical exercise which are matching to the ones obtained from MCS. The figure also presents the fragility curve using a logarithm scale to emphasize the quality of results obtained in the lower tail end. The failure probabilities from the other methods illustrated in this study yield significant error, however, RS-HDMR performs relatively better in the low p_f range. Apart from the MLS-HDMR (with $k = 4$) shown in Fig. 12, $k = 3$ and 5 (n_s = 457 and 913, respectively) are also studied which yield significant inaccuracies in the end results. These results are not produced in this paper to avoid repetition as they are inconsequential to the outcome of this study. A

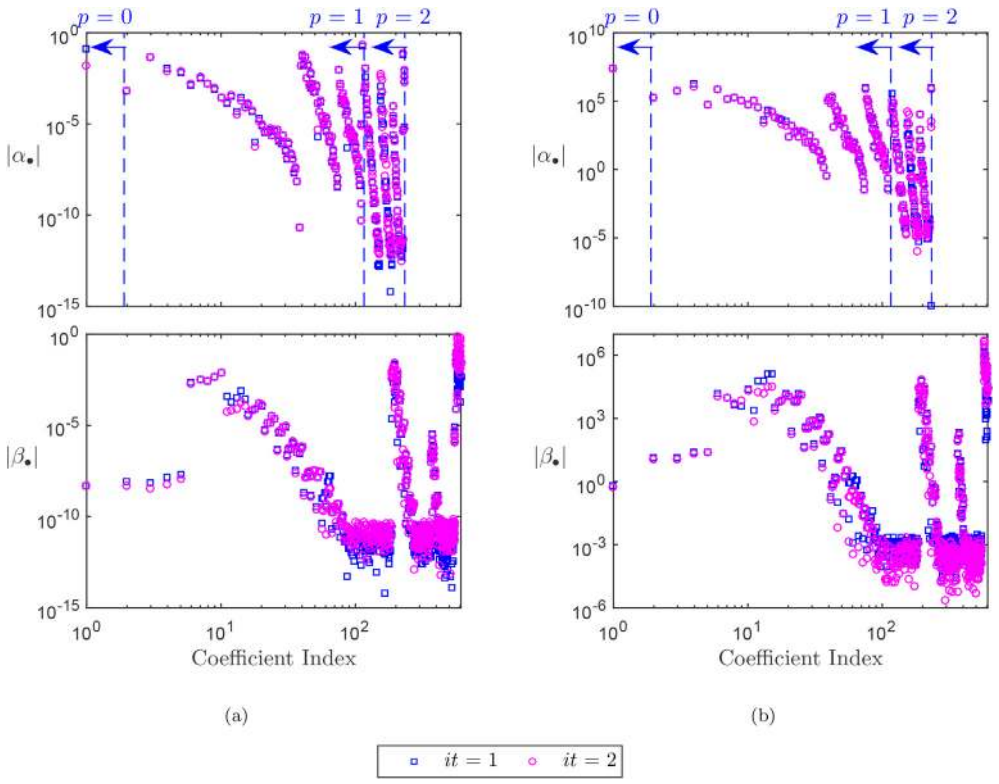

Fig. 11. Magnitude of the unknown coefficients (i.e., $\alpha_\bullet$ and $\beta_\bullet$) associated with PCE and nonparametric terms, respectively, evaluated to determine (a) failure index $\mathfrak{F}$ and (b) σ_1 in the simply supported parallelogram shaped composite plate. For $\alpha_\bullet$, the coefficient indices to the left of the vertical dashed lines correspond terms not larger than the specified degree p of PCE.

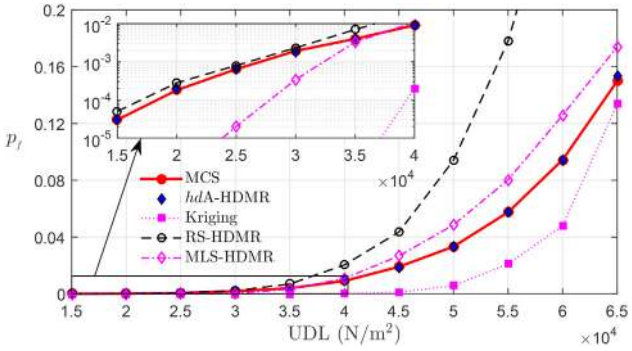

Fig. 12. Fragility curve w.r.t. UDL developed for a simply supported composite plate with [0/90/0] using different methods.

typical illustration of the solved coefficients (i.e. $\alpha_\bullet$ and $\beta_\bullet$) are given in Fig. 13 where the index follows similar sequence as stated in the case of parallelogram composite plate. The plotted results provide similar observations as reported in the previous cases. Moreover, it demonstrates the convergence in the coefficient values (i.e. $\alpha_\bullet$) with successive iterations which also reflect reduction in magnitude of the error modeling coefficient $\beta_\bullet$. Fig. 13a also shows the coefficient $\gamma^{(\bullet)} \in [0, 1]$ which varies based on the location of the realization as it is dependent on the reference point of the iteration and the location where the approximation is evaluated.

The reliability analysis is also performed for the parallelogram shaped M55J/M18 composite plate based on the properties mentioned earlier. The limit state considered for the problem is $g(\mathbf{x}) = 1 - \mathfrak{F}$ which is subjected to UDL of 11 kN/m^2. The probability of failure p_f estimated from different methods is given in Table 2. Once the meta-models are constructed, a simulation size of one million samples is adopted to estimate p_f. Despite this large sample size, Kriging and MLS-HDMR fails to encounter any failure instances. Among these methods, *hd*A-HDMR provides fairly accurate estimation of p_f with limited number of support points. Moreover, the normalized CPU time consumed by different methods is also reported in this study (see Fig. 14) which shows the advantage of the proposed adaptive dimension decomposition. It is performed on an Intel(R) Core(TM) i5-2430 M computer having processing speed and RAM of 2.40 GHz and 6.00 GB, respectively. The software platform adopted to solve this numerical exercise is MATLAB®. This exercise is performed for all the composite plate cases which nearly provide similar findings and thus, the replications of such results are avoided. The proposed method consumes a fraction of time (0.2%) as compared to the direct MCS which nearly consumes 82 h. This is due to the decomposition of the polynomial bases as well as the nonparametric terms which ease the burden on computation. However, direct Kriging application lacks the decomposition of nonparametric terms which leads to more time consumption. Also, MLS based coefficient determination involves independent calculations at each realization which is exhaustive if their number is significant. The adaptive framework of RS-HDMR leads to additional computational cost with more number of support points. In summary, this discussion comprehensively states the merit of the proposed method over the well-known similar tools for reliability analysis.

5.3. Reliability based design optimization

Previous subsections clearly demonstrate the superiority of the proposed method in stochastic computations. Finally, it (i.e. *hd*A-HDMR) is applied to a RBDO problem using the same composite plate. Here, the design problem is solved by evaluating the maximum UDL in trans-

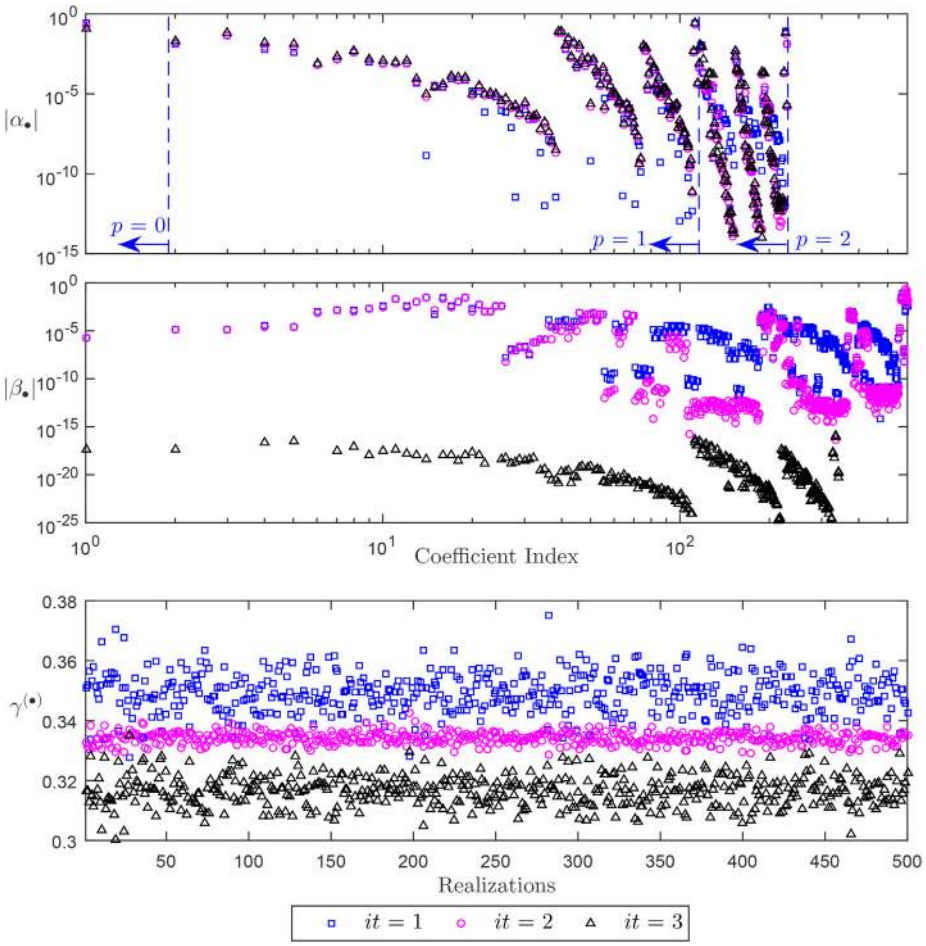

Fig. 13. Magnitude of the unknown coefficients (i.e., $\alpha_\bullet, \beta_\bullet$ and $\gamma^{(\bullet)}$) associated with PCE and nonparametric terms, respectively, evaluated to determine failure index $\mathfrak{F}$ of the simply supported composite plate. For $\alpha_\bullet$, the coefficient indices to the left of the vertical dashed lines correspond terms not larger than the specified degree p of PCE.

Table 2
Probability of failure estimated for the parallelogram shaped composite plate subjected to UDL = 11 kN/m^2.

Method	p_f	Number of function evaluations
Direct MCS	0.000010	1,000,000
*hd*A-HDMR	0.000011	922
Kriging	0.000000	1,000
MLS-HDMR	0.000000	913
RS-HDMR	0.000006	3,000

verse direction for a desired reliability of the carbon-epoxy composite plate. The load is a deterministic variable in this problem of dimension decomposition using random variables as suggested in Eq. (38). The probability of failure is estimated using MCS with a sample size of 5E5. Three different values of desired p_f^* (i.e. 10^{-2}, 10^{-3} and 10^{-4}) are adopted to design the maximum load under the present condition. The UDLs corresponding to these reliabilities are optimized and the results are presented in Fig. 15. The maximum load is also obtained using MCS and it is observed that the results from *hd*A-HDMR are fairly accurate in load estimation. In total the RBDO for case 1 (i.e. $p_f^* = 10^{-2}$), case 2 (i.e. $p_f^* = 10^{-3}$) and case 3 (i.e. $p_f^* = 10^{-4}$) require 930, 930 and 1161 FE calls to convergence. The quality of end results obtained by the proposed method proves to be cost effective for reliability based design optimization. The problems demonstrated above require multiple high-fidelity estimations of the p_f which face notable challenges such as inaccuracies, convergence and computational cost. Also, the results presented here clearly show that other methods discussed previously (e.g. RS-HDMR, MLS-HDMR and Kriging) either lack accuracy, efficiency or both and hence, may not be suitable for large dimensional problems.

6. Summary and conclusions

The present paper proposes an alternative hybrid formulation of the dimension adaptive HDMR. Here, the uncertainty propagation is modeled by multiple generations of the dimension decomposition at different anchored locations. In nutshell, the proposed *hd*A-HDMR performs satisfactorily for problems with a large number of input variables. Different problems are used to demonstrate the advantages of the proposed *hd*A-HDMR. The major contributions in this study are as follows:

1. A novel dimension adaptive formulation is developed using finite difference HDMR, PCE and Gaussian model for error. The support points are judiciously selected in a dimension adaptive sparse grid framework for better accuracy at an optimal computational cost.
2. The error is modeled using a weight function based on the distance between the support points. The associated unknown coefficients are quantified using best linear estimation predictor along with the PCE. Multiple error terms are defined for

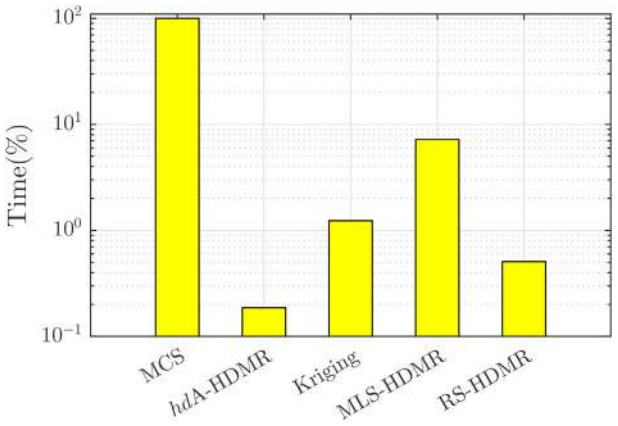

Fig. 14. CPU time consumed by different methods in the reliability analysis of composite plate.

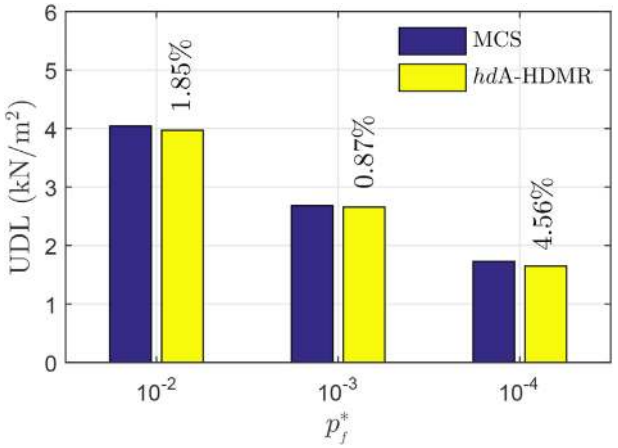

Fig. 15. Design load in UDL estimated for a simply supported composite plate with [0/90/0] from RBDO using the proposed method and MCS for given threshold p_f^*.

component functions in the HDMR using this modeling approach (i.e. hybrid formulation) which has proved to be significantly accurate for stochastic computations.

3. The proposed hybrid dimension adaptive modeling constitutes of mixed-order HDMRs which helps to model uncertainty propagation in case of large dimensional problems (> 100). Three strategies are suggested using the proposed method for different applications such as uncertainty quantification, reliability analysis and RBDO. Overall, it proves to be very effective for high-fidelity modeling as justified by the numerical results, particularly in RBDO where multiple estimations of the probability of failure are required.

CRediT authorship contribution statement

Amit Kumar Rathi: Conceptualization, Methodology, Software, Writing - original draft. **Arunasis Chakraborty:** Conceptualization, Investigation, Supervision, Writing - review & editing.

Declaration of Competing Interest

The authors declare that they have no known competing financial interests or personal relationships that could have appeared to influence the work reported in this paper.

Acknowledgement

Authors wish to acknowledge the anonymous reviewers for their valuable time and suggestions to improve the quality of this article.

Appendix A. Illustration of the Development of Proposed Formulation

The proposed generic formulation of *hd*A-HDMR is illustrated using a low dimensional problem for clarity. For this purpose, a five dimensional problem (i.e. $n = 5$) is considered to demonstrate a 2nd order constitutive equation of HDMR which is expressed by

$$g(\mathbf{x}) = g_0 + \sum_{i=1}^{5} g_i(x_i) + \sum_{i=1}^{4}\sum_{j>i}^{5} g_{ij}(x_i, x_j) + \hat{\mathcal{R}}_2 \tag{A.1}$$

In the above equation, the component functions can be determined using Eq. (3) as

$$\begin{aligned} g_0 = g(\mathbf{c}), \quad g_1(x_1) = g(\mathbf{c}_1, x_1) - g_0, \quad g_2(x_2) = g(\mathbf{c}_2, x_2) - g_0, \\ g_{12}(x_1, x_2) = g(\mathbf{c}_{12}, x_1, x_2) - g_1(x_1) - g_2(x_2) - g_0 \end{aligned} \tag{A.2}$$

and so on for the other indices (i.e. 3, 4 and 5). On substituting these terms back to Eq. (A.1) gives

$$\begin{aligned} g(\mathbf{x}) = {} & g(\mathbf{c}_{12}, x_1, x_2) + g(\mathbf{c}_{13}, x_1, x_3) + g(\mathbf{c}_{14}, x_1, x_4) + g(\mathbf{c}_{15}, x_1, x_5) \\ & + g(\mathbf{c}_{23}, x_2, x_3) + g(\mathbf{c}_{24}, x_2, x_4) \\ & + g(\mathbf{c}_{25}, x_2, x_5) + g(\mathbf{c}_{34}, x_3, x_4) + g(\mathbf{c}_{35}, x_3, x_5) + g(\mathbf{c}_{45}, x_4, x_5) \\ & - 3g(\mathbf{c}_1, x_1) \\ & - 3g(\mathbf{c}_2, x_2) \\ & - 3g(\mathbf{c}_3, x_3) - 3g(\mathbf{c}_4, x_4) - 3g(\mathbf{c}_5, x_5) + 6g(\mathbf{c}) + \hat{\mathcal{R}}_2 \end{aligned} \tag{A.3}$$

This can be illustrated for the full expansion as shown in Fig. 16. The determination of the significant random variables can be performed using the support points evaluated for the 1st order component functions of the HDMR. The sensitivity can be calculated either using Eq. (8) or any other sensitivity analysis [27,28,33,47–49]. In this illustration, let the random variables $x_1, \ldots, x_4$ be significant (i.e. $n_r = 4$) and x_5 as insignificant based on a threshold [36]. The sparse dimension adaptive HDMR formulation can be constructed using Eq. (6) as follows

$$g(\mathbf{x}) = \sum_{i=1}^{3}\sum_{j>1}^{4} g(\mathbf{c}_{ij}, x_i, x_j) - 3\sum_{i=1}^{4} g(\mathbf{c}_i, x_i) + \sum_{j=1}^{5} g(\mathbf{c}_j, x_j) + 2g(\mathbf{c}) + \acute{\mathcal{R}}_2 \tag{A.4}$$

On expanding the above expression as

$$\begin{aligned} g(\mathbf{x}) = {} & g(\mathbf{c}_{12}, x_1, x_2) + g(\mathbf{c}_{13}, x_1, x_3) + g(\mathbf{c}_{14}, x_1, x_4) + g(\mathbf{c}_{23}, x_2, x_3) \\ & + g(\mathbf{c}_{24}, x_2, x_4) + g(\mathbf{c}_{34}, x_3, x_4) \\ & - 2g(\mathbf{c}_1, x_1) - 2g(\mathbf{c}_2, x_2) - 2g(\mathbf{c}_3, x_3) - 2g(\mathbf{c}_4, x_4) \\ & + g(\mathbf{c}_5, x_5) + 2g(\mathbf{c}) + \acute{\mathcal{R}}_2 \end{aligned} \tag{A.5}$$

shows the reduction in number of unknown terms in the dimension decomposition. The approximate surface can be constructed by interpolating each component function using the PCE (i.e. Eq. (7)) as

$$\begin{aligned} \tilde{g}(\mathbf{x}) = {} & y_{12}(\mathbf{c}_{12}, x_1, x_2) + y_{13}(\mathbf{c}_{13}, x_1, x_3) + y_{14}(\mathbf{c}_{14}, x_1, x_4) \\ & + y_{23}(\mathbf{c}_{23}, x_2, x_3) + y_{24}(\mathbf{c}_{24}, x_2, x_4) \\ & + y_{34}(\mathbf{c}_{34}, x_3, x_4) - 2y_1(\mathbf{c}_1, x_1) - 2y_2(\mathbf{c}_2, x_2) \\ & - 2y_3(\mathbf{c}_3, x_3) - 2y_4(\mathbf{c}_4, x_4) + y_5(\mathbf{c}_5, x_5) + 2y_0 \end{aligned} \tag{A.6}$$

where, the terms

$$y_i = \alpha_0\Gamma_0 + \alpha_i\Gamma_1(z_i) + \alpha_{ii}\Gamma_2(z_i, z_i) + \cdots + \sum_{k=1}^{n_s} \beta_k R_i(\mathbf{z}, \mathbf{z}^k) \tag{A.7}$$

and

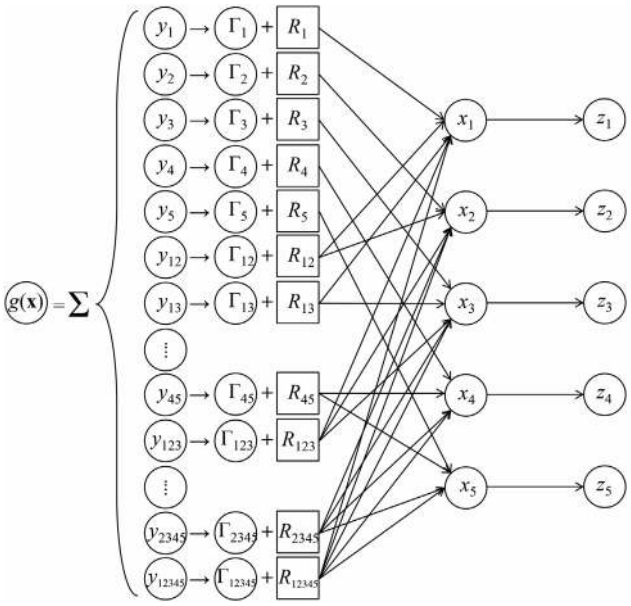

Fig. 16. A schematic illustration of full dimension decomposition expansion providing the correspondence between the key variables for $n = 5$.

$$\begin{aligned} y_{ij} = \; & \alpha_0\Gamma_0 + \alpha_i\Gamma_1(z_i) + \alpha_j\Gamma_1(z_j) + \alpha_{ii}\Gamma_2(z_i,z_i) + \alpha_{ij}\Gamma_2(z_i,z_j) \\ & + \alpha_{jj}\Gamma_2(z_j,z_j) + \cdots \\ & + \sum_{k=1}^{n_s}\beta_k R_{ij}(\mathbf{z},\mathbf{z}^k) \end{aligned} \tag{A.8}$$

Further, simplifying these terms give

$$\begin{aligned} y_i &= (\alpha_0 - \alpha_{ii}) + \alpha_i z_i + \alpha_{ii}z_i^2 + \cdots + \sum_{k=1}^{n_s}\beta_k R_i(\mathbf{z},\mathbf{z}^k) \\ \Rightarrow y_i &= \alpha_0' + \alpha_i z_i + \alpha_{ii}z_i^2 + \cdots + \sum_{k=1}^{n_s}\beta_k R_i(\mathbf{z},\mathbf{z}^k) \end{aligned} \tag{A.9}$$

$$\begin{aligned} y_{ij} &= (\alpha_0 - \alpha_{ii} - \alpha_{jj}) + \alpha_i z_i + \alpha_j z_j + \alpha_{ii}z_i^2 + \alpha_{ij}z_i z_j \\ &\quad + \alpha_{jj}z_j^2 + \cdots + \sum_{k=1}^{n_s}\beta_k R_{ij}(\mathbf{z},\mathbf{z}^k) \\ \Rightarrow y_{ij} &= \alpha_0' + \alpha_i z_i + \alpha_j z_j + \alpha_{ii}z_i^2 + \alpha_{ij}z_i z_j + \alpha_{jj}z_j^2 \\ &\quad + \cdots + \sum_{k=1}^{n_s}\beta_k R_{ij}(\mathbf{z},\mathbf{z}^k) \end{aligned} \tag{A.10}$$

Substituting these terms in Eqs. (A.7) and (A.8) back to Eq. (A.6) leads to the dimension decomposition formulation as

$$\begin{aligned} \tilde{g}(\mathbf{x}) = \; & \boldsymbol{\Gamma}_{12}(x_1,x_2)^{\mathrm{T}}\boldsymbol{\alpha}_{12}^* + \boldsymbol{\Gamma}_{13}(x_1,x_3)^{\mathrm{T}}\boldsymbol{\alpha}_{13}^* + \boldsymbol{\Gamma}_{14}(x_1,x_4)^{\mathrm{T}}\boldsymbol{\alpha}_{14}^* \\ & + \boldsymbol{\Gamma}_{23}(x_2,x_3)^{\mathrm{T}}\boldsymbol{\alpha}_{23}^* + \boldsymbol{\Gamma}_{24}(x_2,x_4)^{\mathrm{T}}\boldsymbol{\alpha}_{24}^* \\ & + \boldsymbol{\Gamma}_{34}(x_3,x_4)^{\mathrm{T}}\boldsymbol{\alpha}_{34}^* - 2\boldsymbol{\Gamma}_1(x_1)^{\mathrm{T}}\boldsymbol{\alpha}_1^* - 2\boldsymbol{\Gamma}_2(x_2)^{\mathrm{T}}\boldsymbol{\alpha}_2^* \\ & - 2\boldsymbol{\Gamma}_3(x_3)^{\mathrm{T}}\boldsymbol{\alpha}_3^* - 2\boldsymbol{\Gamma}_4(x_4)^{\mathrm{T}}\boldsymbol{\alpha}_4^* + \boldsymbol{\Gamma}_5(x_5)^{\mathrm{T}}\boldsymbol{\alpha}_5^* \\ & + \mathbf{r}_{12}(x_1,x_2)^{\mathrm{T}}\boldsymbol{\beta}_{12}^* + \mathbf{r}_{13}(x_1,x_3)^{\mathrm{T}}\boldsymbol{\beta}_{13}^* + \mathbf{r}_{14}(x_1,x_4)^{\mathrm{T}}\boldsymbol{\beta}_{14}^* \\ & + \mathbf{r}_{23}(x_2,x_3)^{\mathrm{T}}\boldsymbol{\beta}_{23}^* + \mathbf{r}_{24}(x_2,x_4)^{\mathrm{T}}\boldsymbol{\beta}_{24}^* \\ & + \mathbf{r}_{34}(x_3,x_4)^{\mathrm{T}}\boldsymbol{\beta}_{34}^* - 2\mathbf{r}_1(x_1)^{\mathrm{T}}\boldsymbol{\beta}_1^* - 2\mathbf{r}_2(x_2)^{\mathrm{T}}\boldsymbol{\beta}_2^* - 2\mathbf{r}_3(x_3)^{\mathrm{T}}\boldsymbol{\beta}_3^* \\ & - 2\mathbf{r}_4(x_4)^{\mathrm{T}}\boldsymbol{\beta}_4^* + \mathbf{r}_5(x_5)^{\mathrm{T}}\boldsymbol{\beta}_5^* \\ & + 2\boldsymbol{\alpha}_0^* \end{aligned} \tag{A.11}$$

In the above expression, the unknown coefficients $\boldsymbol{\alpha}$ and $\boldsymbol{\beta}$ are determined using Eqs. (16) and (19), respectively. It may be noted that in the determination of individual sets of $\boldsymbol{\alpha}$ and $\boldsymbol{\beta}$ different support points are used. This is based on the support points associated with the respective random variables generated using the proposed sparse grid scheme as per Eq. (21). Hence, this offers a judicious division of the support points which makes it more attractive than RS-HDMR and Kriging. On simplifying the expansion, the hybrid formulation of the proposed dimension decomposition is expressed as

$$\begin{aligned} \tilde{g}(\mathbf{x}) = \; & \alpha_{0,12} + \alpha_{1,12}\Gamma_1(z_1) + \alpha_{2,12}\Gamma_1(z_2) + \alpha_{11,12}\Gamma_2(z_1,z_1) \\ & + \alpha_{12,12}\Gamma_2(z_1,z_2) + \alpha_{22,12}\Gamma_2(z_2,z_2) \\ & + \alpha_{0,13} + \alpha_{1,13}\Gamma_1(z_1) + \alpha_{3,13}\Gamma_1(z_3) + \alpha_{11,13}\Gamma_2(z_1,z_1) \\ & + \alpha_{13,13}\Gamma_2(z_1,z_3) + \alpha_{33,13}\Gamma_2(z_3,z_3) + \cdots \\ & - 2\alpha_{0,1} - 2\alpha_{1,1}\Gamma_1(z_1) - 2\alpha_{11,1}\Gamma_2(z_1,z_1) - 2\alpha_{0,2} \\ & - 2\alpha_{2,2}\Gamma_1(z_2) - 2\alpha_{22,2}\Gamma_2(z_2,z_2) - \cdots \\ & - 2\alpha_{44,4}\Gamma_2(z_4,z_4) + \alpha_{0,5} + \alpha_{5,1}\Gamma_1(z_5) + \alpha_{55,5}\Gamma_2(z_5,z_5) \\ & + \mathbf{r}_{12}(x_1,x_2)^{\mathrm{T}}\boldsymbol{\beta}_{12}^* + \mathbf{r}_{13}(x_1,x_3)^{\mathrm{T}}\boldsymbol{\beta}_{13}^* + \mathbf{r}_{14}(x_1,x_4)^{\mathrm{T}}\boldsymbol{\beta}_{14}^* \\ & + \mathbf{r}_{23}(x_2,x_3)^{\mathrm{T}}\boldsymbol{\beta}_{23}^* + \mathbf{r}_{24}(x_2,x_4)^{\mathrm{T}}\boldsymbol{\beta}_{24}^* \\ & + \mathbf{r}_{34}(x_3,x_4)^{\mathrm{T}}\boldsymbol{\beta}_{34}^* - 2\mathbf{r}_1(x_1)^{\mathrm{T}}\boldsymbol{\beta}_1^* - 2\mathbf{r}_2(x_2)^{\mathrm{T}}\boldsymbol{\beta}_2^* \\ & - 2\mathbf{r}_3(x_3)^{\mathrm{T}}\boldsymbol{\beta}_3^* - 2\mathbf{r}_4(x_4)^{\mathrm{T}}\boldsymbol{\beta}_4^* + \mathbf{r}_5(x_5)^{\mathrm{T}}\boldsymbol{\beta}_5^* + 2\boldsymbol{\alpha}_0^* \end{aligned} \tag{A.12}$$

Hence, using the above expression to construct the multi HDMR based response surface, the proposed formulation (Eq. (15)) can be expressed in the following form

$$\begin{aligned} \tilde{g}(\mathbf{x}) = \; & \gamma^{(1)}(\mathbf{x},\mathbf{c}^{(1)})\Big[\alpha_{0,12}^{(1)} + \alpha_{1,12}^{(1)}\Gamma_1^{(1)}(z_1) + \alpha_{2,12}^{(1)}\Gamma_1^{(1)}(z_2) + \alpha_{11,12}^{(1)}\Gamma_2^{(1)}(z_1,z_1) \\ & + \alpha_{12,12}^{(1)}\Gamma_2^{(1)}(z_1,z_2). \quad + \alpha_{22,12}^{(1)}\Gamma_2^{(1)}(z_2,z_2) + \cdots + \alpha_{44,34}^{(1)}\Gamma_2^{(1)}(z_3,z_4) - 2\alpha_{0,1}^{(1)} \\ & - 2\alpha_{1,1}^{(1)}\Gamma_1^{(1)}(z_1) - 2\alpha_{11,1}^{(1)}\Gamma_2^{(1)}(z_1,z_1) - \cdots \quad - 2\alpha_{44,4}^{(1)}\Gamma_2^{(1)}(z_4,z_4) + \alpha_{0,5}^{(1)} \\ & + \alpha_{5,1}^{(1)}\Gamma_1^{(1)}(z_5) + \alpha_{55,5}^{(1)}\Gamma_2^{(1)}(z_5,z_5) + \mathbf{r}_{12}^{(1)}(x_1,x_2)^{\mathrm{T}}\boldsymbol{\beta}_{12}^{*(1)} + \cdots \\ & + \mathbf{r}_{34}^{(1)}(x_3,x_4)^{\mathrm{T}}\boldsymbol{\beta}_{34}^{*(1)} - 2\mathbf{r}_1^{(1)}(x_1)^{\mathrm{T}}\boldsymbol{\beta}_1^{*(1)} - \cdots - 2\mathbf{r}_4^{(1)}(x_4)^{\mathrm{T}}\boldsymbol{\beta}_4^{*(1)} \\ & + \mathbf{r}_5^{(1)}(x_5)^{\mathrm{T}}\boldsymbol{\beta}_5^{*(1)} + 2\boldsymbol{\alpha}_0^{*(1)}\Big] \\ & + \sum_{i=2}^{it}\gamma^{(i)}(\mathbf{x},\mathbf{c}^{(i)})\Big[\alpha_{0,1}^{(i)} + \alpha_{1,1}^{(i)}\Gamma_1^{(i)}(z_1) + \alpha_{11,1}^{(i)}\Gamma_2^{(i)}(z_1,z_1) + \cdots \\ & + \alpha_{44,4}^{(i)}\Gamma_2^{(i)}(z_4,z_4) + \mathbf{r}_1^{(i)}(x_i)^{\mathrm{T}}\boldsymbol{\beta}_1^{*(i)} + \cdots + \mathbf{r}_4^{(i)}(x_4)^{\mathrm{T}}\boldsymbol{\beta}_4^{*(i)} + 3\boldsymbol{\alpha}_0^{*(i)}\Big] \end{aligned} \tag{A.13}$$

In Eq. (A.13) the unknown weight coefficient $\gamma^{(i)}$ associated with the multiple generation of HDMR can be evaluated using Eq. (20).

References

[1] Wang GG, Shan S. Review of metamodeling techniques in support of engineering design optimization. J Mech Des 2007;129(4):370–80.
[2] Wang H, Tang L, Li G. Adaptive MLS-HDMR metamodeling techniques for high dimensional problems. Expert Syst Appl 2011;38(11):14117–26.
[3] Dey S, Mukhopadhyay T, Adhikari S. Metamodel based high-fidelity stochastic analysis of composite laminates: A concise review with critical comparative assessment. Compos Struct 2017;171:227–50.
[4] Kleijnen JP. Regression and kriging metamodels with their experimental designs in simulation: a review. Eur J Oper Res 2017;256(1):1–16.
[5] Xiu D, Karniadakis GE. Modeling uncertainty in flow simulations via generalized polynomial chaos. J Comput Phys 2003;187(1):137–67.
[6] Ernst OG, Mugler A, Starkloff H-J, Ullmann E. On the convergence of generalized polynomial chaos expansions. ESAIM: M2AN 2012;46(2):317–39.
[7] Isukapalli SS. Uncertainty analysis of transport-transformation models, Ph.D. dissertation, Rutgers, The State University of New Jersey; 1999..
[8] Li D-Q, Jiang S-H, Cheng Y-G, Zhou C-B. A comparative study of three collocation point methods for odd order stochastic response surface method. Struct Eng Mech 2013;45(5):595–611.
[9] Sudret B, Kiureghian AD. Comparison of finite element reliability methods. Prob Eng Mech 2002;17(4):337–48.
[10] Blatman G, Sudret B. Sparse polynomial chaos expansions and adaptive stochastic finite elements using a regression approach. C R Méc 2008;336(6):518–23.
[11] Li D, Chen Y, Lu W, Zhou C. Stochastic response surface method for reliability analysis of rock slopes involving correlated non-normal variables. Comput Geotech 2011;38:58–68.
[12] Xiong F, Chen W, Xiong Y, Yang S. Weighted stochastic response surface method considering sample weights. Struct Multidiscip Optim 2011;43(6):837–49.
[13] Xiong F, Liu Y, Xiong Y, Yang S. A double weighted stochastic response surface method for reliability analysis. J Mech Sci Technol 2012;26(8):2573–80.
[14] Rathi AK, Sharma S, P. V, Chakraborty A. Sequential stochastic response surface method using moving least squares based sparse grid scheme for efficient

reliability analysis, International J Comput Methods 2018;15(3):1840017 [Online Ready]. doi:110.1142/S0219876218400170..
[15] Blatman G, Sudret B. Reliability and optimization of structural systems, CRC Press; 2010 [Ch. Reliability analysis of a pressurized water reactor vessel using sparse polynomial chaos expansions, pp. 9–16]..
[16] Hu C, Youn BD. Adaptive-sparse polynomial chaos expansion for reliability analysis and design of complex engineering systems. Struct Multidiscip Optim 2011;43(3):419–42.
[17] Schobi R, Sudret B, Wiart J. Polynomial-chaos-based Kriging. Int J Uncertain Quantification 2015;5(2):171–93.
[18] Schobi R, Sudret B, Marelli S. Rare event estimation using polynomial-chaos kriging. ASCE-ASME J Risk Uncertain Eng Syst Part A Civil Eng 2017;3(2): D4016002.
[19] Dutta S, Ghosh S, Inamdar MM. Optimisation of tensile membrane structures under uncertain wind loads using PCE and kriging based metamodels. Struct Multidiscip Optim 2018;57(3):1149–61.
[20] Zhang L, Lu Z, Wang P. Efficient structural reliability analysis method based on advanced Kriging model. Appl Math Model 2015;39(2):781–93.
[21] Haeri A, Fadaee MJ. Efficient reliability analysis of laminated composites using advanced Kriging surrogate model. Compos Struct 2016;149:26–32.
[22] Chowdhury R, Rao BN, Prasad AM. High-dimensional model representation for structural reliability analysis. Commun Numer Methods Eng 2009;25(4):301–37.
[23] Aliş ÖF, Rabitz H. Efficient implementation of high dimensional model representations. J Math Chem 2001;29(2):127–42.
[24] Sobol' I. Theorems and examples on high dimensional model representation. Reliab Eng Syst Saf 2003;79(2):187–93.
[25] Rahman S, Xu H. A univariate dimension-reduction method for multi-dimensional integration in stochastic mechanics. Prob Eng Mech 2004;19(4):393–408.
[26] Xu H, Rahman S. Decomposition methods for structural reliability analysis. Prob Eng Mech 2005;20(3):239–50.
[27] Ziehn T, Tomlin A. GUI-HDMR – a software tool for global sensitivity analysis of complex models. Environ Model Softw 2009;24(7):775–85.
[28] Dey S, Mukhopadhyay T, Adhikari S. Stochastic free vibration analysis of angle-ply composite plates - A RS-HDMR approach. Compos Struct 2015;122(4):526–36.
[29] Chowdhury R, Adhikari S. High dimensional model representation for stochastic finite element analysis. Appl Math Model 2010;34(12):3917–32.
[30] Dey S, Mukhopadhyay T, Spickenheuer A, Adhikari S, Heinrich G. Bottom up surrogate based approach for stochastic frequency response analysis of laminated composite plates. Compos Struct 2016;140:712–27.
[31] Chakraborty S, Chowdhury R. Towards 'h-p adaptive' generalized ANOVA. Comput Methods Appl Mech Eng 2017;320:558–81.
[32] Chen C, Hu D, Liu Q, Han X. Evaluation on the interval values of tolerance fit for the composite bolted joint. Compos Struct 2018;206:628–36.
[33] Ma X, Zabaras N. An adaptive high-dimensional stochastic model representation technique for the solution of stochastic partial differential equations. J Comput Phys 2010;229(10):3884–915.
[34] Rao BN, Chowdhury R, Prasad AM. High dimensional model representation for piece-wise continuous function approximation. Commun Numer Methods Eng 2008;24(12):1587–609.
[35] Chowdhury R, Rao B, Prasad A. Stochastic sensitivity analysis using HDMR and score function. Sadhana 2009;34(6):967–86.
[36] Rathi AK, Chakraborty A. Dimension adaptive finite difference decomposition using multiple sparse grids for stochastic computation. Struct Saf 2018;75:119–32.
[37] Yadav V, Rahman S. A hybrid polynomial dimensional decomposition for uncertainty quantification of high-dimensional complex systems. Prob Eng Mech 2014;38:22–34.
[38] García-Macías E, Castro-Triguero R, Friswell MI, Adhikari S, Sáez A. Metamodel-based approach for stochastic free vibration analysis of functionally graded carbon nanotube reinforced plates. Compos Struct 2016;152:183–98.
[39] Chakraborty S, Chowdhury R. Moment independent sensitivity analysis: H-PCFE–based approach. J Comput Civil Eng 2017;31(1):06016001.
[40] Chakraborty S, Chowdhury R. An efficient algorithm for building locally refined hp-adaptive H-PCFE: application to uncertainty quantification. J Comput Phys 2017;351:59–79.
[41] Chakraborty S, Chowdhury R. Hybrid framework for the estimation of rare failure event probability. J Eng Mech 2017;143(5):04017010.
[42] Chakraborty S, Majumder D. Hybrid reliability analysis framework for reliability analysis of tunnels. J Comput Civil Eng 2018;32(4):04018018.
[43] Chatterjee T, Chowdhury R. An efficient sparse Bayesian learning framework for stochastic response analysis. Struct Saf 2017;68:1–14.
[44] Chatterjee T, Chowdhury R. Refined sparse Bayesian learning configuration for stochastic response analysis. Prob Eng Mech 2018;52:15–27.
[45] Ulaganathan S, Couckuyt I, Dhaene T, Degroote J, Laermans E. High dimensional kriging metamodelling utilising gradient information. Appl Math Model 2016;40 (9):5256–70.
[46] Rabitz H, Aliş ÖF, Shorter J, Shim K. Efficient input-output model representations. Comput Phys Commun 1999;117(1–2):11–20.
[47] Ziehn T, Tomlin AS. A global sensitivity study of sulfur chemistry in a premixed methane flame model using HDMR. Int J Chem Kinet 2008;40(11):742–53.
[48] Ziehn T, Tomlin A. Global sensitivity analysis of a 3D street canyon model–Part I: The development of high dimensional model representations. Atmos Environ 2008;42(8):1857–73.
[49] Benson J, Ziehn T, Dixon NS, Tomlin AS. Global sensitivity analysis of a 3D street canyon model–Part II: Application and physical insight using sensitivity analysis. Atmos Environ 2008;42(8):1874–91.
[50] Ditlevsen O, Madsen HO. Structural reliability methods. Chichester, UK: John Wiley & Sons Inc.; 1996.
[51] Liu PL, Kiureghian AD. Multivariate distribution models with prescribed marginals and covariances. Prob Eng Mech 1986;1(2):105–12.
[52] Jia G, Taflanidis AA. Kriging metamodeling for approximation of high-dimensional wave and surge responses in real-time storm/hurricane risk assessment. Comput Methods Appl Mech Eng 2013;261–262:24–38.
[53] Cressie NAC. Statistics for spatial data. revised ed. New York, USA: John Wiley & Sons Ltd.; 1993.
[54] Xue G, Dai H, Zhang H, Wang W. A new unbiased metamodel method for efficient reliability analysis. Struct Saf 2017;67:1–10.
[55] Mukhopadhyay T, Chakraborty S, Dey S, Adhikari S, Chowdhury R. A critical assessment of Kriging model variants for high-fidelity uncertainty quantification in dynamics of composite shells. Arch Comput Methods Eng 2017;24(3):495–518.
[56] Klimke A, Wohlmuth B. Computing expensive multivariate functions of fuzzy numbers using sparse grids. Fuzzy Sets Syst 2005;154(3):432–53.
[57] Reddy JN. Mechanics of laminated composite plates and shells: theory and analysis. Boca Raton, FL, USA: CRC Press; 2004.
[58] Matthies HG, Brenner CE, Bucher CG, Soares CG. Uncertainties in probabilistic numerical analysis of structures and solids-stochastic finite elements. Struct Saf 1997;19(3):283–336.
[59] Ghanem RG, Spanos PD. Stochastic finite elements: a spectral approach. 1st ed. New York: Springer-Verlag; 1991.
[60] Sasikumar P, Suresh R, Gupta S. Analysis of CFRP laminated plates with spatially varying non-Gaussian inhomogeneities using SFEM. Compos Struct 2014;112:308–26.
[61] Chen NZ, Soares CG. Spectral stochastic finite element analysis for laminated composite plates. Comput Methods Appl Mech Eng 2008;197(51–52):4830–9.
[62] Nocedal J, Wright SJ. Numerical optimization, 2nd ed., Springer Series in Operations Research. New York, USA: Springer Verlag; 2006..
[63] MATLAB, version 7.13.0.564 (R2011b), The MathWorks Inc., Natick, Massachusetts; 2011..
[64] Lophaven SN, Nielsen HB, Søndergaard J. DACE: A MATLAB kriging toolbox, version 2.0, Tech. Rep. IMM-TR-2002-12, Informatics and Mathematical Modelling (IMM), Technical University of Denmark (August 2002)..